Modelling the role of enzymatic pathways in the metabolism of docosahexaenoic acid by monocytes and its association with osteoarthritic pain
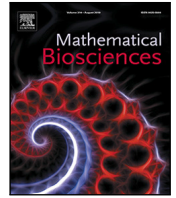
Article

Published Version

the End User Agreement.

www.reading.ac.uk/centaur

CentAUR

Central Archive at the University of Reading

Reading's research outputs online

Contents lists available at ScienceDirect

Mathematical Biosciences

Original Research Article

Modelling the role of enzymatic pathways in the metabolism of docosahexaenoic acid by monocytes and its association with osteoarthritic pain

S.J. Franks [a,*], P.R.W. Gowler [c,d], J.L. Dunster [b], J. Turnbull [d,e,f], S.A. Gohir [e], A. Kelly [e], A.M. Valdes [c,e], J.R. King [a], D.A. Barrett [e,f], V. Chapman [c,d,e], S. Preston [a]

[a] School of Mathematical Sciences, University of Nottingham, Nottingham, NG7 2RD, UK
[b] Institute for Cardiovascular and Metabolic Research, University of Reading, UK
[c] Pain Centre Versus Arthritis, University of Nottingham Medical School, Queen's Medical Centre, Nottingham, UK
[d] School of Life Sciences, Faculty of Medicine and Health Sciences, University of Nottingham, Nottingham, UK
[e] NIHR Nottingham Biomedical Research Centre, University of Nottingham, Nottingham, UK
[f] Centre for Analytical Bioscience, Advanced Materials and Healthcare Technologies Division, School of Pharmacy, University of Nottingham, Nottingham, UK

A R T I C L E   I N F O

A B S T R A C T

Chronic pain is a major cause of disability and suffering in osteoarthritis (OA) patients. Endogenous specialised pro-resolving molecules (SPMs) curtail pro-inflammatory responses. One of the SPM intermediate oxylipins, 17-hydroxydocasahexaenoic acid (17-HDHA, a metabolite of docosahexaenoic acid (DHA)), is significantly associated with OA pain. The aim of this multidisciplinary work is to develop a mathematical model to describe the contributions of enzymatic pathways (and the genes that encode them) to the metabolism of DHA by monocytes and to the levels of the down-stream metabolites, 17-HDHA and 14-hydroxydocasahexaenoic acid (14-HDHA), motivated by novel clinical data from a study involving 30 participants with OA. The data include measurements of oxylipin levels, mRNA levels, measures of OA severity and self-reported pain scores.

We propose a system of ordinary differential equations to characterise associations between the different datasets, in order to determine the homeostatic concentrations of DHA, 17-HDHA and 14-HDHA, dependent upon the gene expression of the associated metabolic enzymes. Using parameter-fitting methods, local sensitivity and uncertainty analysis, the model is shown to fit well qualitatively to experimental data.

The model suggests that up-regulation of some ALOX genes may lead to the down-regulation of 17-HDHA and that dosing with 17-HDHA increases the production of resolvins, which helps to down-regulate the inflammatory response. More generally, we explore the challenges and limitations of modelling real data, in particular individual variability, and also discuss the value of gathering additional experimental data motivated by the modelling insights.

1. Introduction

Inflammation plays an essential role in tissue repair and in protecting the body from further tissue injury. This process involves the localised up-regulation of pro-inflammatory signalling molecules, including cytokines, that attract neutrophils to the area of injury. At later stages of the response, specialised pro-resolving mediators (SPMs) are generated within the cells and actively down-regulate the immune response to curtail pro-inflammatory signalling ensuring the return to tissue homeostasis [1]. The SPMs are oxylipins, produced by the oxygenation of polyunsaturated fatty acids (PUFAs) by cyclooxygenases, lipoxygenases and cytochrome P450s [2,3]. Agile pro-inflammatory and resolution responses depend upon the rapid up- and down-regulation of a complex pathway of genes (occurring on a timescale of days/weeks), which are controlled by transcription factors such as NF-κB, allowing the rapid change in levels of messenger RNA (mRNA) and in functional responses [4–6].

The most well characterised SPMs derived from DHA, the resolvins (Rvs), protectins (PDs) and maresins (MaRs), have been shown to halt the transition from acute to chronic inflammation preventing pathogenesis [7]. The SPMs suppress cytokine production and resolve destructive

---

* Corresponding author.
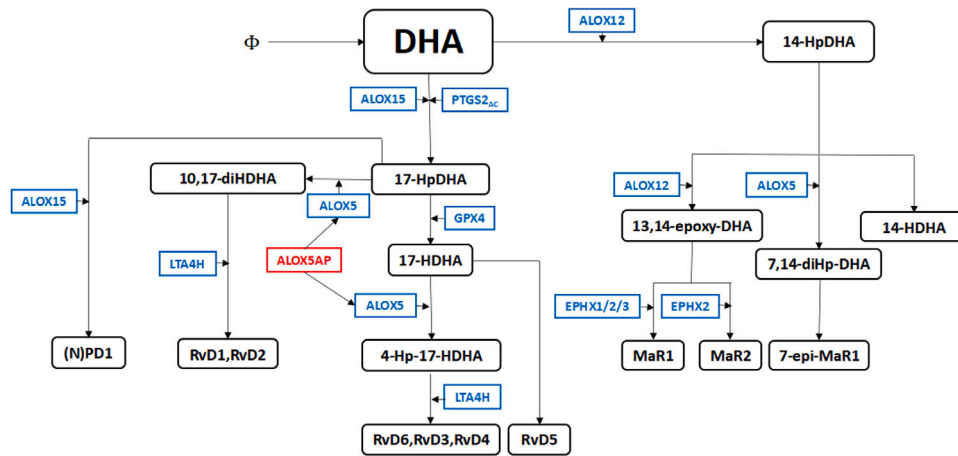 *E-mail address:* susan.franks@nottingham.ac.uk (S.J. Franks).

Fig. 1. The metabolism of DHA into its downstream products, simplified from the Atlas of Inflammation Resolution tool [12]. The black boxes are bioactive oxylipins, the blue boxes are the genes that are associated with the enzymes that metabolise the oxylipins and the red boxes are genes which activate other genes. Arrows without enzymes indicate that the oxylipin breaks down naturally by auto-oxidation.

inflammation by regulating leukocyte trafficking and clearance of inflammatory mediators [8,9]. Dysfunction in the processes that underlie the switch from pro-inflammatory signalling to resolution may result in the sustained inflammation and pathogenesis seen in chronic diseases including Alzheimer's, cardiovascular diseases and arthritis diseases, including OA [10].

There are two series of resolvins (D and E), which are produced from the omega-3 PUFAs docosahexaenoic acid (DHA) and eicosapentaenoic acid (EPA), respectively [1]. 17-hydroxydocasahexaenoic acid (17-HDHA) is a precursor of the D-series resolvins, which is readily transported outside of the cells, making it detectable in biofluids including blood plasma and serum via liquid chromatography tandem mass spectrometry (LC-MS/MS) [11]. The metabolism of DHA and its downstream products is shown in Fig. 1 based on a simplification of the pathway described in [12]. Note that other variations of this pathway have been proposed in [13,14]. The contribution of any feedback loops regulating the inflammatory mediators is currently unknown.

Past studies have shown that plasma levels of 17-HDHA are negatively correlated with self-reported pain in people with osteoarthritis (OA), and that higher levels of 17-HDHA are associated with higher thresholds to thermal stimulus in healthy volunteers [11]. The link between 17-HDHA and OA pain was further strengthened by the demonstration that exogenous administration of 17-HDHA inhibited pain responses in rodent models of OA pain [15]. Although the exact cell populations/types which contribute to the production of 17-HDHA are unknown, the numbers of circulating monocytes is altered in OA patients [16]. In addition, monocytes had increased expression of activation markers in OA, which is associated with pain and inflammation [16], suggesting they are a likely cell type contributing to the plasma levels of 17-HDHA.

A gap in our knowledge is an understanding of the relationship between the expression of the genes that encode the enzymes involved in the synthesis/catabolism of the SPMs and their levels in plasma. To address this, here we develop a novel quantitative model to capture for the first time the metabolism of DHA, incorporating all the disparate experimental datasets, in order to explore the relationships between gene expression and oxylipin concentration. We use the model to predict levels of oxylipins in the blood and to determine what happens when individuals are dosed with 17-HDHA. The model seeks to be at a level of complexity appropriate to the nature of the biological components and available data.

In the following section we introduce and summarise the data from the clinical study. In Section 3 we devise a mathematical model to characterise the time evolution of DHA, 14-hydroxydocasahexaenoic acid (14-HDHA) and 17-HDHA concentrations. Section 4 then addresses

Table 1

Descriptive characteristics of study cohort. BMI = body mass index; K/L grade = Kellgren–Lawrence radiographic grade; NRS = numerical rating scale; IQR = interquartile range.

Cohort	
n	30
Sex F	60%
Age median (IQR)	63 (11.25)
BMI kg/m^2 median (IQR)	30.1 (5.43)
K/L grade 0| 1	2	3 |4	0| 12	10	7 |1
NRS pain score median (IQR)	5 (3)

how model parameters are fitted to the clinical data and how the model is used to explore the relationship between gene expression and oxylipin concentrations and to examine the effect of downstream products, namely the D-series resolvins, after dosing with 17-HDHA.

2. Study participants and biological data

2.1. Study design

Baseline blood samples were collected from a cohort of n = 30 participants diagnosed with OA [17], defined by X-ray severity of pathology (Kellgren–Lawrence (KL) radiographic grade) and numerical rating scale (NRS) pain score. Ethical approval was obtained from the Research Ethics Committee (ref: 18/EM/0154) and the Health Research Authority (protocol no: 18021). The descriptive characteristics of the participants are summarised in Table 1.

The KL grade is a clinician assigned integer score from 0–4, where KL = 0 corresponds to no pathological features and KL = 4 to the presence of large osteophytes, marked narrowing of joint space, severe sclerosis, and definite deformity of bone ends. The numerical rating scale (NRS) pain score is a patient reported score of perceived pain intensity between 0 and 10, where 0 represents no pain, and 10 represents severe pain.

Oxylipins were measured in plasma prepared from the whole blood and monocytes were isolated from the whole blood to measure gene expression. One measurement for each patient was performed.

2.2. Levels of DHA and metabolites

Participants fasted for 12 h before blood collection to minimise any effects of inter-individual dietary variations on DHA concentrations and downstream metabolites. Levels of DHA, 17-HDHA and 14-HDHA were measured in plasma using LC-MS/MS and the standard methodology for
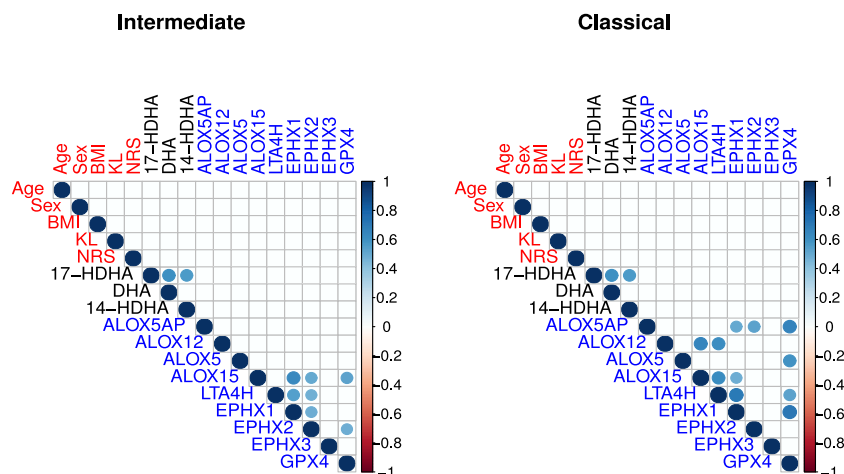
Fig. 2. The correlation of oxylipin plasma concentrations (denoted by the black labels) with patient characteristics (denoted by the red labels) and genes (denoted by the blue labels) expressed from intermediate and classical monocytes. Positive correlations are displayed in blue where the colour intensity and the area of the circle are proportional. Only correlations where the significance level p<0.01 are plotted.

Table 2

Median concentrations and IQR of DHA (docohexadecanoic acid), 17-HDHA (17-hydroxy DHA) and 14-HDHA (14-hydroxy DHA).

Plasma oxylipins	Median (IQR)
DHA (μM)	33.66 (21.58)
17-HDHA (nM)	0.42 (0.88)
14-HDHA (nM)	2.7 (2.71)

their quantification is described in [18,19]. A summary of the resulting measured plasma concentrations of oxylipins that appear in the DHA pathway is provided in Table 2. Concentrations of resolvins, maresins and protectins were below the lower limit of quantification (i.e. < 50 pM, 10 pM and 50 pM, respectively) so were not measurable in our samples.

One participant was an outlier in the study (identified using Grubbs test), having significantly higher levels of 14-HDHA (22.14 nM compared to the median of 2.7 nM). No specific reason was found for the high level but it was noted that this individual was the only one taking a combination of NSAIDs, steroids and opioids. This individual was removed from the dataset used for the model.

2.3. Gene expression dataset

The plasma oxylipin concentrations measured experimentally reflect the overall circulating concentrations from multiple in-vivo and dietary sources. Monocytes are a likely important cell source of the plasma oxylipin molecules [20] so were isolated from the whole blood and sorted by fluorescence-activated cell sorting (FACS) into two populations, intermediate and classical [21], defined by relative expression levels of CD14 and CD16 surface proteins. Classical monocytes comprise the majority of circulating monocytes and are highly phagocytic. Intermediate monocytes comprise about 2%–8% of circulating monocytes and their functions include production of reactive oxygen species (ROS), antigen presentation, participating in the proliferation and stimulation of T cells, inflammatory responses and angiogenesis [22].

In order to measure the expression of genes involved in the DHA pathway, total RNA was extracted from the cell suspensions of the classical and intermediate monocytes and next-generation RNA sequencing was performed by Genewiz. The SMART-Seq v4 Ultra Low Input RNA Kit (Clontech) was used to perform cDNA synthesis and amplification. Illumina-compatible sequencing libraries were constructed and then sequenced on the Illumina HiSeq 2500 with a 2 × 150 paired-end configuration. The quality of raw counts was assessed using FASTQC

and reads were subsequently trimmed to remove adapter sequence and low quality nucleotide calls using Trimmomatic v.0.36. STAR aligner v.2.5.2b was used to map the trimmed reads to the ENSEMBL Homo sapiens GRCh38 genome. Unique gene hit counts were obtained through the featureCounts tool of the Subread package v.1.5.2 with only unique reads falling within exon regions counted.

mRNA levels were quantified as the number of reads that map to each gene which is proportional to the level of mRNA, sequencing depth, gene length and RNA composition. Using the raw count data for the two monocyte populations, we normalised the counts using the median of ratios method (described in [23]) to scale the raw count values for sequencing depth and RNA composition, to provide datasets allowing a comparison of gene expression between samples. Given that we are comparing counts between participants for the same gene, we did not need to normalise for gene length.

Expression levels of the genes for the key enzymatic pathways involved in the metabolism of DHA are summarised in Table 3. Median values of EPHX1 are higher and ALOX5AP and ALOX12 lower, in classical monocytes with the remaining genes having similar levels for the two monocyte populations. The interquartile ranges for ALOX5AP, EPHX1 and GPX4 are larger for classical monocytes indicating greater variation in individuals.

2.4. Correlations between lipids, gene expression and clinical measurements

For initial exploratory analysis of the clinical data we computed the pairwise Pearson correlation coefficients between plasma concentrations of DHA, 17-HDHA and 14-HDHA, gene expression and patient characteristics i.e. age, sex, BMI, pain score (NRS) and osteoarthritis score (KL).

Concentrations of 17-HDHA were correlated with both DHA and 14-HDHA, but there was little correlation between oxylipin concentrations and age, BMI, sex or NRS score and, similarly, between mRNA expression and patient characteristics (Fig. 2). 17-HDHA and 14-HDHA are likely correlated because they are both metabolites of DHA (rather than there being a particular biological relationship between them). This implies that DHA metabolism down both the ALOX12 and ALOX15 pathways is consistent as the DHA concentration changes i.e. the conversion ratio to 17-HDHA and 14-HDHA is the same, regardless of any increases in the DHA concentration.

There were also correlations between the mRNA expression of genes with each other, particularly in the classical monocytes (Fig. 2). For both populations, ALOX15 was correlated with GPX4. However, for intermediate monocytes, ALOX15 was also correlated with EPHX1 and

Table 3
Normalised raw gene count data from intermediate and classical monocytes with the associated enzymes encoded with these genes.

| Gene	Enzyme (abbreviation)	Normalised gene count	
		Intermediate median (IQR)	Classical median (IQR)
ALOX5	Arachidonate 5-lipoxygenase (5-LOX)	18 (12)	6 (9)
ALOX12	Arachidonate 12-lipoxygenase (12-LOX)	260 (156)	138 (162)
ALOX15	Arachidonate 15-lipoxygenase (15-LOX)	27 (30)	25 (44)
ALOX5AP	5-Lipoxygenase activating protein (FLAP)	2690 (1062)	2287 (1565)
LTA4H	Leukotriene-A(4) hydrolase (LTA4H)	50 (38)	54 (75)
EPHX1	Microsomal Epoxide Hydrolase 1 (EPHX1)	1325 (781)	2445 (1344)
EPHX2	Microsomal Epoxide Hydrolase 2 (EPHX2)	17 (15)	22 (12)
EPHX3	Microsomal Epoxide Hydrolase 3 (EPHX3)	4 (13)	3 (4)
GPX4	Glutathione peroxidase 4 (GPX4)	1797 (333)	2002 (1175)
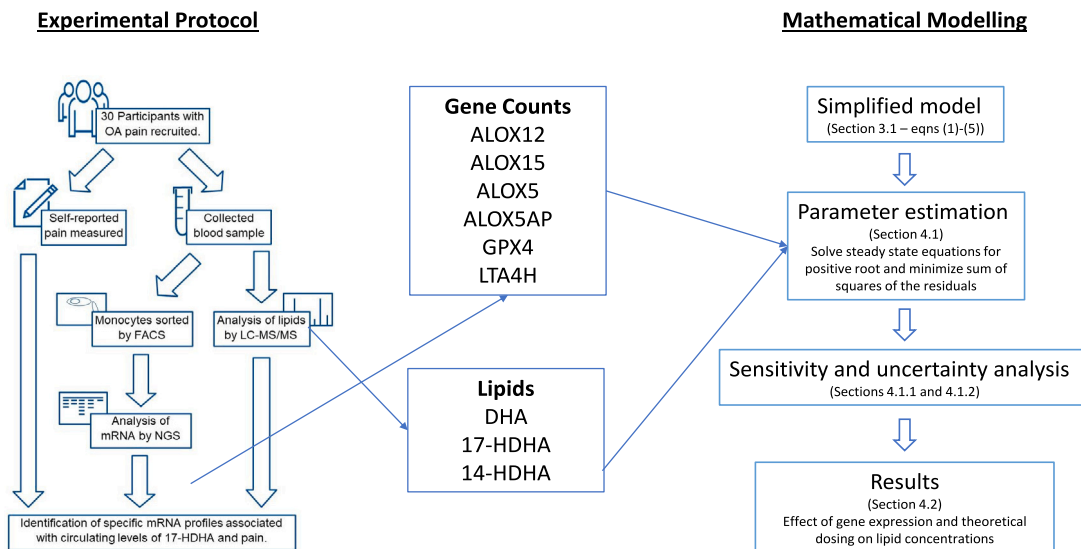
Fig. 3. A summary of the relationship between the experimental protocol and the modelling process. In the centre boxes are the genes and oxylipins relevant to the DHA pathway that have been measured experimentally and used in the mathematical model.

EPHX2, whereas in classical monocytes, it was also correlated with LTA4H and EPHX3. ALOX12 was correlated with GPX4 and EPHX3 and ALOX5 with ALOX5AP and LTA4H for classical monocytes. LTA4H was correlated with EPHX1 and EPHX2 and GPX4 with EPHX2 for intermediate monocytes and for classical monocytes, LTA4H is correlated with GPX4 and EPHX1 and GPX4 also with EPHX1.

In the following sections, we consider both the intermediate and classical monocytes individually, and also combined to model the oxylipin concentration. The concentration of oxylipins is made up of contributions from both populations of monocytes, along with other cells including platelets and other leukocytes. However, the relative contributions from these different cell types are unknown, so we only consider monocytes in this paper and assume that they are the major contributor. This can be modified when more information becomes available.

In a fixed volume of blood taken from participants, the ratio of the median number of classical to intermediate monocytes was approximately 13:1. However, the ratio of the median amount of RNA extracted from these cells was approximately 6:4, indicating that the amount of RNA extracted is not correlated with cell number. We therefore assume that the latter gives a better indication of relative contributions as not all cells will be metabolising DHA and expressing relevant genes. RNAseq was performed on a fixed amount of RNA from each monocyte type, so assuming that one molecule of RNA in the classical makes the same contribution as one molecule of RNA in the intermediate and also that one molecule of RNA in classical or intermediate in patient y contributes the same amount of one molecule

RNA in patient x, we calculate the combined gene expression from both monocyte populations ("total monocyte gene count") to be a 60% contribution from the normalised gene counts obtained from classical and 40% from intermediate monocytes.

3. Model formulation and parameterisation

3.1. The model

In Section 2 we summarised the different sets of data that have been collected from our cohort of participants. Analysis of pairwise correlations did not identify any significant linear relationships between individual genes and plasma oxylipin levels. However, a linear correlation may not be expected if it is a combination of genes that determines the concentration of the oxylipins via a nonlinear dynamic process. We therefore employ mathematical modelling techniques to characterise associations between the different datasets in order to reveal how differences in gene expression may explain the plasma levels of DHA and its metabolites. A summary of the modelling process presented in the following sections and of how we use the experimental data is provided in Fig. 3.

We begin by simplifying the pathway diagram presented in Fig. 1 to focus on the precursors upstream of 17-HDHA and 14-HDHA to determine what influences their levels. These simplifying assumptions should not have any impact on the overall pathway as the rates of loss of our main metabolites remain unchanged. However, it will have the benefit of making it easier to identify parameter values (discussed in
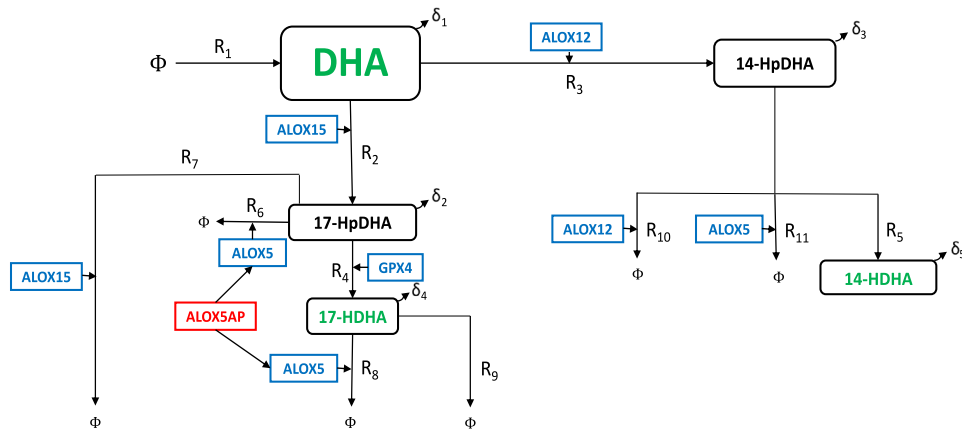
Fig. 4. The metabolism of DHA into its downstream products where the black boxes are bioactive oxylipins, the blue boxes are the genes that are associated with the enzymes that metabolise the oxylipins and the red boxes are genes which drive the key genes. Arrows without enzymes indicate that the oxylipin breaks down naturally by auto-oxidation. Oxylipin names in green denote those that were measured in plasma in this study. The rates at which the oxylipins are metabolised are denoted by R_i and the natural oxylipin degradation rate constants are denoted by δ_i for $i = 1, \ldots, 11$.

Sections 3.3 and 4.1). A system of ordinary differential equations describing the time evolution of each bioactive oxylipin in the simplified pathway diagram (Fig. 4) and their interactions with other metabolites is presented below.

We define the concentration of oxylipins in these equations to be the average concentration per unit total volume, i.e. both the internal V_i (in monocytes) and external V_e (in plasma) volumes. Assuming equilibrium between the internal and external concentrations, the effective rate constants are the actual internal rate constants multiplied by $V_i/(V_i + \mu V_e)$ where μ is the relevant partition coefficient i.e. [oxylipin]$_e = \mu$[oxylipin]$_i$. The actual internal concentration is then a multiple $(V_i + V_e)/(V_i + \mu V_e)$ of the variables appearing in Eqs. (1)–(5). This approach is applied to DHA and also its metabolites, which are all exchanged between the plasma and monocytes.

Enzymes encoded with associated genes are responsible for each step in the biochemical metabolic pathway and the rate terms (defined in Tables 4–6) are therefore dependent upon the concentration of active enzyme. The production of enzymes is complicated and their concentration could not be measured experimentally in this study. However, we do have the mRNA levels of the corresponding genes but it is important to note that the relationship between the mRNA levels and the protein (and therefore activity) is complex and likely to depend on the state of the local environment. The main aim of this study was to advance our understanding of how differences in participant gene expression may relate to their corresponding plasma levels of DHA and its metabolites. Given that mRNA is degraded in the cytoplasm, which can be regulated at different stages of transcription and translation, the ratio of RNA to subsequent protein is not precisely known. Nevertheless, an increase in the expression of mRNA is usually indicative of an increase in the protein [24]. As these samples are from people with chronic OA pain of varying levels it is likely that the current environment reflects a long-term state change, which we assume to be the same for all of the enzymes in the pathway. Although the relationships between the mRNA and protein levels are influenced by local availability of substrates, this is likely to be comparable for all of the enzymes considered in this model as the local environment is similar for all (i.e. all are from the same population of cells) [25]. We therefore adopt the simplifying assumption that the model and its rate constants k, in the equations below, encompass the complicated relationship between the enzyme activity and corresponding gene expression. Gene expression is assumed to be the normalised gene counts for each individual from intermediate, classical or total (defined earlier) monocytes.

Table 4
Rate terms for the metabolism of DHA to 14-HpDHA and 17-HpDHA expressed in Eq. (1). [ ] denotes the bioactive oxylipin concentration and rate constants are denoted by k.

Rate	Description	Term
R_1	Production of DHA from diet	P_{DHA}
R_2	Conversion by 15-LOX of DHA to 17-HpDHA	k_2ALOX15[DHA]
R_3	Conversion by 12-LOX of DHA to 14-HpDHA	k_3ALOX12[DHA]

DHA

DHA is an omega-3 PUFA that is obtained mainly from the diet at rate R_1 (Fig. 4) where R_1 is related to the dietary intake of free fatty acids and the rate at which they are converted to DHA. DHA can also be produced intracellularly by the continuous recycling of fatty acyl chains from phospholipids [26,27] but this is very slow compared to dietary contributions so we do not consider it here. DHA can cross cell membranes and is metabolised to various specialised pro-resolving mediators (SPMs) mostly within cells.

DHA is metabolised in the cell into 14-HpDHA by 12-LOX (associated gene ALOX12) at rate R_3 and 17-HpDHA by 15-LOX (associated gene ALOX15) at rate R_2. Note that gene expression can also be affected by diet but this is not considered here. The equation describing the concentration of DHA is thus

$$\frac{d[\text{DHA}]}{dt} = R_1 - R_2 - R_3 - \delta_1[\text{DHA}], \tag{1}$$

where we assume that DHA decays with rate constant δ_1 and the conversion of DHA by 12-LOX and 15-LOX to 14-HpDHA and 17-HpDHA follows mass action kinetics. We make this assumption to limit the number of unknown parameters in the model. The reaction terms are listed in Table 4.

15-LOX is expressed in many different cells and has important roles in the metabolism of PUFAs to a wide range of physiologically and pathologically relevant products [28,29]. In Fig. 1, aspirin acetylated COX-2 also contributes to the metabolism of DHA to 17-HpDHA in conjunction with 15-LOX. However, no participants in the clinical study were taking aspirin so we have not included this term in the present model. 12-LOX oxidises PUFAs, particularly omega-6 and 3 fatty acids, to generate a number of bioactive oxylipin metabolites. A number of studies have revealed the importance of 12-LOX in oxidative and inflammatory responses [30–32].

The metabolism of DHA is essentially modular with the two main sections, the ALOX12 pathway and the ALOX15 pathway, not known to interact with each other (Fig. 4). The equations representing the oxylipin metabolism in each section are detailed below.
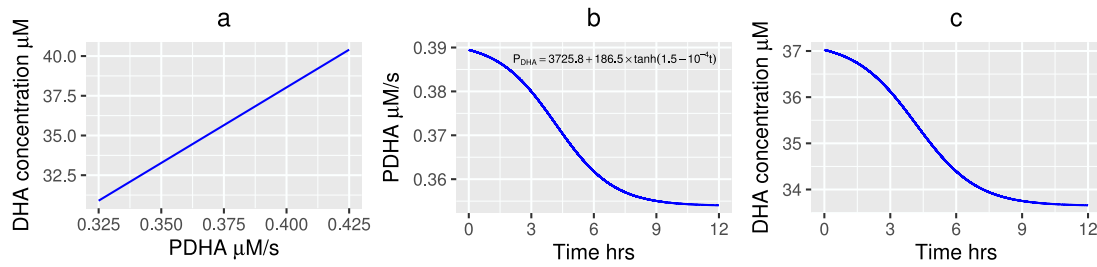
Fig. 5. Model simulations illustrating the relationship between the parameter P_{DHA} and the concentration of DHA (left), the assumed gradual decrease in P_{DHA} during fasting (middle) and the decrease in the DHA concentration during a 12 h fast (right), using the median mRNA values from our cohort for intermediate monocytes and parameter values given in Table 8.

Table 5

Rate terms expressed in Eqs. (2)–(3). [ ] denotes the oxylipin concentration and rate constants are denoted by k.

Rate	Description	Term
R_{10}	Conversion of 14-HpDHA by 12-LOX	k_{10}ALOX12[14-HpDHA]
R_{11}	Conversion of 14-HpDHA by 5-LOX	k_{11}ALOX5[14-HpDHA]
R_5	Conversion of 14-HpDHA to 14-HDHA	k_5[14-HpDHA]

ALOX12 pathway

DHA is metabolised by 12-LOX to 14-HpDHA. This is then metabolised by 12-LOX and 5-LOX (associated gene ALOX5) to produce Maresins and auto-oxidised to produce 14-HDHA, all of which play an important role in the resolution of inflammation by reducing neutrophil chemotaxis, platelet aggregation and increasing phagocytosis in leukocytes [33]. The equations representing the concentrations of 14-HpHDA and 14-HDHA are:

$$\frac{d[\text{14-HpDHA}]}{dt} = R_3 - R_{10} - R_{11} - R_5 - \delta_3[\text{14-HpDHA}], \quad (2)$$

$$\frac{d[\text{14-HDHA}]}{dt} = R_5 - \delta_5[\text{14-HDHA}], \quad (3)$$

where the reaction terms are listed in Table 5.

ALOX15 pathway

17-HpDHA is converted into 17-HDHA by GPX4 (associated gene GPX4) at rate R_4. It is also converted by 5-LOX, activated by FLAP (encoded by the ALOX5AP gene) at rate R_6 and by 15-LOX at rate R_7. We assume that the natural decay rate constants for 17-HpDHA and 17-HDHA are δ_2 and δ_4, respectively. 17-HDHA is then metabolised by 5-LOX (activated by FLAP) and auto-oxidised to the D-series resolvins at rates R_8 and R_9, respectively. This is discussed in more detail in Section 4.2.2.

The equations representing the concentrations of 17-HpDHA and 17-HDHA are

$$\frac{d[\text{17-HpDHA}]}{dt} = R_2 - R_4 - R_6 - R_7 - \delta_2[\text{17-HpDHA}], \quad (4)$$

$$\frac{d[\text{17-HDHA}]}{dt} = R_4 - R_8 - R_9 - \delta_4[\text{17-HDHA}], \quad (5)$$

where the reaction terms are listed in Table 6.

Fasting and initial conditions

Participants in the cohort fasted before blood collection to minimise inter-individual variations in recent dietary intake. In [34], it was shown that in free fatty acids, the clearance of exogenous DHA takes only a few hours to return to its homeostatic level. This suggests that following a 12 h fast, as adopted in this study, levels of DHA and its metabolites are at steady state. During this time, mRNA levels remain unchanged as any dietary effects at the protein or gene level will occur over a timescale of days.

We first consider the effect of fasting on the oxylipin concentrations by solving the system of ODEs given by (1)–(5) using the parameter values described later (except P_{DHA}) and the median mRNA values in

our cohort for intermediate monocytes. P_{DHA} encompasses the dietary intake of free fatty acids and the rate at which they are converted to DHA so we vary this parameter to illustrate its effect on the oxylipin concentrations. We assume initially at $t = 0$, the oxylipin concentrations are

$$[\text{DHA}]_0 = 0, \quad [\text{17-HpDHA}]_0 = 0, \quad [\text{17-HDHA}]_0 = 0, \quad [\text{14-HpDHA}]_0 = 0,$$

$$[\text{14-HDHA}]_0 = 0, \quad (6)$$

where $[\ ]_0$ is the initial concentration of oxylipin, and run the simulations until a steady state has been reached for each value of P_{DHA} ranging from 0.325–0.425 μM/s. The dose response curve for the resulting steady state concentration of DHA is shown in Fig. 5a. The concentration of DHA increases linearly with P_{DHA} (note that this model does not account for the body storing (and accessing) excess DHA in tissue or in its esterified form) and similar relationships are observed between both 17-HDHA and 14-HDHA and P_{DHA}.

In [35] it was shown that the concentration of DHA and EPA in their control cohort decreased by approximately 10% following at least 10 h of fasting. This small decrease illustrates the body's homeostatic function to maintain the levels of essential compounds such as fatty acids to sustain the availability of DHA until bodily reserves are exhausted, which takes weeks. We therefore assume that initially, prior to fasting, the concentration of DHA is 10% higher than the measured median steady state value in the cohort and the corresponding value of P_{DHA} is determined from Fig. 5a. We solve Eqs. (1)–(5) with these new set of initial conditions and assume that the rate at which DHA is produced by the diet, decreases from this new value to the value previously calculated at steady state over a 12 h period as shown in Fig. 5b. As DHA and P_{DHA} are linearly related, this functional form has been chosen based on the reduction of DHA observed in [35].

Fig. 5c illustrates the time evolution of the DHA levels during this 12 h of fasting. The concentration profile of DHA (and similarly for 17-HDHA and 14-HDHA, not shown) decreases rapidly over the first 6 h before attaining steady state towards the end of the fasting period.

In the following sections, we exploit the steady state behaviour of the mRNA values and oxylipin concentrations to solve the steady state equations given in Section 3.2.

3.2. Steady state equations

As discussed previously, we assume that the bioactive oxylipin concentrations and mRNA levels measured experimentally are the values at steady state. The complex stereochemistry involved in the production of 17-HDHA and SPMs is thought to be mainly auto-oxidative or enzyme dependent [36,37]. In the absence of any other information, and with the aim of keeping the number of parameters to a minimum, we therefore assume that the decay rate constants of the intermediate oxylipins are negligible i.e. $\delta_1 = \delta_2 = \delta_3 = \delta_4 = 0$.

At steady state i.e. $\frac{d}{dt} = 0$, Eqs. (1)–(5) can be reduced to the following algebraic system

$$P_{DHA_M} = k_{2_M}\text{ALOX15}_M[\text{DHA}] + k_{3_M}\text{ALOX12}_M[\text{DHA}], \quad (7)$$

Table 6

Rate terms expressed in Eqs. (4)–(5). [ ] denotes the oxylipin concentration, rate constants are denoted by k and K_A is a constant.

Rate	Description	Term
R_4	Conversion by GPX4 of 17-HpDHA to 17-HDHA	k_4GPX4[17-HpDHA]
R_6	Conversion of 17-HpDHA by 5-LOX (activated by FLAP)	$k_6(1 + \frac{\text{ALOX5AP}}{K_A})$ALOX5[17-HpDHA]
R_7	Conversion of 17-HpDHA by 15-LOX	k_7ALOX15[17-HpDHA]
R_8	Conversion of 17-HDHA by 5-LOX (activated by FLAP)	$k_8(1 + \frac{\text{ALOX5AP}}{K_A})$ALOX5[17-HDHA]
R_9	Conversion of 17-HDHA by auto-oxidation	k_9[17-HDHA]

$$0 = k_{3_M}\text{ALOX12}_M[\text{DHA}] - k_{10_M}\text{ALOX12}_M[\text{14-HpDHA}]$$
$$- k_{5_M}[\text{14-HpDHA}] - k_{11_M}\text{ALOX5}_M[\text{14-HpDHA}], \quad (8)$$

$$0 = k_{5_M}[\text{14-HpDHA}] - \delta_{5_M}[\text{14-HDHA}], \quad (9)$$

$$0 = k_{2_M}\text{ALOX15}_M[\text{DHA}] - k_{4_M}\text{GPX4}_M[\text{17-HpDHA}]$$
$$- k_{7_M}\text{ALOX15}_M[\text{17-HpDHA}]$$
$$- k_{6_M}\text{ALOX5}_M\left(1 + \frac{\text{ALOX5AP}_M}{K_{A_M}}\right)[\text{17-HpDHA}], \quad (10)$$

$$0 = k_{4_M}\text{GPX4}_M[\text{17-HpDHA}]$$
$$- k_{8_M}\text{ALOX5}_M\left(1 + \frac{\text{ALOX5AP}_M}{K_{A_M}}\right)[\text{17-HDHA}]$$
$$- k_{9_M}[\text{17-HDHA}], \quad (11)$$

where subscript M denotes the monocyte type I (intermediate), C (classical) and T (total).

We introduce a statistical model to represent the experimentally measured oxylipin concentrations $\mathbf{y}_i^{data}$ for individual i in terms of the model steady state solution $\mathbf{y}_i = f(\theta_i)$ and an error term ϵ_i (as the data does not match up precisely with the model solutions) so that

$$\mathbf{y}_i^{data} = f(\theta_i) + \epsilon_i.$$

Here $\mathbf{y}_i^{data}$ and $\mathbf{y}_i$ are given, respectively, by the vector ([DHA]$_i$, [17-HpDHA]$_i$, [17-HDHA]$_i$, [14-HpDHA]$_i$, [14-HDHA]$_i$)^T of observed and modelled concentrations, and θ_i is the collection of unknown parameters P_{DHA_M}, k_{l_M} for $l = 2 - 11$, K_{A_M} and the decay rate constant δ_{5_M} for the ith individual.

3.3. Model parameter values

We separately examine each monocyte population, i.e. intermediate and classical, as well as the combined population, and identify parameter values for each type based on the expression of genes measured in the clinical data.

The parameters in the model have not been measured directly in this study and are not well documented in existing literature. However, [13] has estimated Michaelis–Menten parameters for 12-LOX and 15-LOX in platelets acting on the substrate DHA *in vitro* and the steady state kinetic values are given in Table 7. The values in Table 7 include estimated uncertainty measured in [13] via ± standard error, though henceforth we use the point estimates.

As mentioned earlier, reactions have been modelled linearly to reduce the number of unknown parameters needing to be determined. However, from our cohort, the concentrations of DHA range from 16.19–63.65 μM suggesting from Table 7, that the reactions of 15-LOX and 12-LOX with DHA are both saturated by DHA and the linear approach assumed is inconsistent with the kinetic data. However, adopting Michaelis–Menten or saturated forms for R_2 and R_3 gives a worse fit between predicted and measured concentrations as discussed in Appendix A. Therefore, given the uncertainty regarding the currently unknown factors involved in converting enzyme concentrations into the

Table 7

Steady state kinetic values of 15-LOX (also known as h15-LOX-2) and 12-LOX (also known as h12-LOX) with substrate DHA taken from Tables 1 and 6 in [13] measured *in vitro*. Assumed values of k_{2_M} and k_{3_M} used in the simulations calculated from Eq. (12) where [DHA] is the median concentration in the cohort and $k_{cat_{12}}$, $K_{m_{12}}$, $k_{cat_{15}}$, $K_{m_{15}}$ are the steady state kinetic values taken from [13] for 12-LOX and 15-LOX, respectively.

Enzyme	Substrate	k_{cat} (s^{-1})	K_m (μM)	Value used in simulations
15-LOX	DHA	3 ± 0.3	11 ± 2	$k_{2_M} = 6.72 \times 10^{-6}$ s^{-1}
12-LOX	DHA	14 ± 1	1.1 ± 0.2	$k_{3_M} = 4.03 \times 10^{-5}$ s^{-1}

mRNA levels, in addition to differences between *in vitro* and *in vivo* kinetic values and between cell types i.e. platelets vs. monocytes, we assume that the rate constants k_2 and k_3 in Eq. (1) are determined by

$$k_{2_M} = \frac{k_{cat_{15}}\alpha_{15}}{K_{m_{15}} + [\text{DHA}]_m}, \qquad k_{3_M} = \frac{k_{cat_{12}}\alpha_{12}}{K_{m_{12}} + [\text{DHA}]_m}, \quad (12)$$

so that the reactions can be modelled linearly without making any assumptions regarding the relative magnitudes of the substrate concentration and Michaelis constant. In the absence of any other information, we assume that these values are the same for the two populations of monocytes. Here α_{12} and α_{15} are the proportionality constants relating the active enzyme concentration to its corresponding gene expression, $k_{cat_{12}}$, $K_{m_{12}}$, $k_{cat_{15}}$, $K_{m_{15}}$ are given by the k_{cat} and K_m values in Table 7 for 12-LOX and 15-LOX, respectively, and [DHA]$_m$ is the median concentration of DHA measured in our cohort as given in Table 2 i.e. 33.66 μM. For simplicity we assume that $\alpha_{12} = \alpha_{15} = 1 \times 10^{-4}$ with units μM to give appropriate timescales. However, we explore when $\alpha_{12} \neq \alpha_{15}$ by varying k_{2_M} and k_{3_M} independently in the uncertainty analysis in Section 4.1.2. Similar equations for other oxylipin substrates and enzyme concentrations are assumed, but as we do not have any information regarding the Michaelis–Menten constants and turnover numbers, the fitted values determined in Section 4.1 are representative of the values which would be obtained by calculating in this manner.

P_{DHA_M} is a very important parameter in the pathway as it determines the concentration of DHA and ultimately the remaining metabolites. It represents the rate of production of DHA from the diet and other sources, which is likely to vary between individuals in our cohort. We therefore determine its value directly from the steady state Eq. (7) using the measured concentration of DHA and values for ALOX12 and ALOX15 for each individual in the cohort and the values of k_{2_M} and k_{3_M} in Table 7 so that

$$[\text{DHA}] = \frac{P_{DHA_M}}{k_{2_M}\text{ALOX15}_M + k_{3_M}\text{ALOX12}_M}, \quad (13)$$

confirming that DHA is proportional to its intake P_{DHA} as observed in Fig. 5a.

In the following subsection, we fit by least squares the remaining parameters in the model using the measured oxylipin concentrations for DHA, 17-HDHA and 14-HDHA and imposing non-negativity constraints on all parameters whereby $\theta_i \geq 0$.

Table 8

Fitted parameter values determined from the steady state equations (7)–(11). Values for P_{DHA} denote min–max (median) calculated from Eq. (13) using values of k_{2_M} and k_{3_M} given in Table 7 and measured concentrations of DHA and gene expressions of ALOX15 and ALOX12 from each individual in the cohort.

Parameter	Fitted value			Units
	Intermediate	Classical	Total	
P_{DHA_M}	0.15–0.92 (0.37)	0.02–0.84 (0.2)	0.11–0.84 (0.27)	μM s^{-1}
k_{2_M}	0.0672×10^{-4}	0.0672×10^{-4}	0.0672×10^{-4}	s^{-1}
k_{3_M}	0.403×10^{-4}	0.403×10^{-4}	0.403×10^{-4}	s^{-1}
k_{4_M}	2.2×10^{-9}	1.1×10^{-9}	1×10^{-9}	s^{-1}
k_{5_M}	1.2×10^{-8}	1.66×10^{-8}	1.7×10^{-8}	s^{-1}
k_{6_M}	3.5×10^{-9}	3.68×10^{-8}	1×10^{-9}	s^{-1}
k_{7_M}	27.46×10^{-4}	27.73×10^{-4}	24.6×10^{-4}	s^{-1}
k_{8_M}	1×10^{-9}	1.47×10^{-9}	1.03×10^{-9}	s^{-1}
k_{9_M}	9×10^{-4}	4.99×10^{-4}	5.13×10^{-4}	s^{-1}
k_{10_M}	0.51×10^{-4}	0.76×10^{-4}	0.79×10^{-4}	s^{-1}
k_{11_M}	1.94×10^{-4}	1.85×10^{-4}	1.87×10^{-4}	s^{-1}
K_{A_M}	1	1	1	Constant
δ_{5_M}	1×10^{-4}	1×10^{-4}	1×10^{-4}	s^{-1}

4. Predictive results

4.1. Global parameter estimation

We assume that individuals have parameters in common, so that $\theta_i = \theta$, and wish to determine an optimal set of parameter values $\theta = \hat{\theta}$ which minimise an objective function we specify as the weighted sum of squares of the residuals between the model simulations and measured data

$$S(\theta) = \sum_{i=1}^{n} \sum_{j}^{m} W_j \times (y_{ij} - y_{ij}^{data})^2. \tag{14}$$

Here j represents the number of measured bioactive oxylipins, W_j are the weights which are assumed to be equal to the reciprocal of the standard deviation of the observed data, y_{ij} are the calculated oxylipin concentrations for each individual from the steady state Eqs. (8)–(11), y_{ij}^{data} are the corresponding experimentally measured concentrations, n is the number of individuals and m is the number of equations.

To obtain $f(\theta_i)$, Eqs. (8)–(11) were solved for the positive root of the steady state oxylipin concentration using the multiroot function in R which employs the Newton–Raphson method. The residuals were then calculated and the bobyqa function (which employs a trust region method that forms quadratic models by interpolation) used to determine the parameters which minimise the sum of squares of the residuals. Non-negativity constraints are used as lower limits but no upper limits are imposed. No other *a-priori* assumptions are made.

The parameters k_{5_M} and δ_{5_M} are related by Eq. (9) so the steady state values are essentially multiples of the actual parameters but the multiplying factors are unknown. We therefore assume a value for δ_{5_M} and fit for k_{5_M} using the method described. We also assume a constant value for K_{A_M} which is the same for all monocyte types. This can be modified when more information becomes available. The fitted values for each monocyte type are summarised in Table 8 using the measured mRNA levels for each individual.

The concentrations of DHA, 17-HDHA and 14-HDHA calculated from solving the system of algebraic Eqs. (7)–(11) for each individual using these common steady state parameter values, the median value of P_{DHA_M} and the gene expression for each individual in our cohort is shown in Fig. 6 for each monocyte type.

There is some qualitative agreement between the best obtained approximation of the globally optimal fit of the steady state concentrations and the experimental values. mRNA levels and their corresponding fitted parameters from intermediate monocytes give the best fit overall (i.e. the objective function is minimised) so we will use these values going forward and drop the subscript M. However, it should be noted that total monocytes give a slightly better fit for 17-HDHA.

The model tends to underestimate the oxylipin concentrations for some individuals who have large measured DHA, 14-HDHA and 17-HDHA concentrations indicating that some of the assumptions we have made for the model and parameters are not capturing the full behaviour.

In Fig. 2, we observed a correlation in the cohort between the measured concentrations of 17-HDHA and DHA and also between 17-HDHA and 14-HDHA. These relationships are plotted in Fig. 7 along with the corresponding model predictions which also indicate some linear correlation between these oxylipins.

4.1.1. Sensitivity analysis

To determine the most important parameters in our model, we perform a local sensitivity analysis to analyse the effect of changing the individual parameters on the oxylipin concentration. Choosing the average mRNA levels across our cohort and using the fitted parameter values in Table 8 with the median value chosen for P_{DHA}, we solve our steady state system of Eqs. (7)–(11) to determine the oxylipin concentrations. We then estimate the local effect of parameters on these steady states by increasing and decreasing each individually by 10% and calculating the relative change in our output variable in relation to the relative change in parameter i.e.

$$\frac{\Delta \mathbf{y}/\mathbf{y}}{|\Delta \theta|/\theta}$$

where $\Delta\theta = 1.1 \times \theta$ and $\Delta\theta = 0.9 \times \theta$. This gives the relative sensitivities providing a measure of how much the concentration of DHA, 14-HDHA and 17-HDHA increase or decrease in relation to an up- or down-regulation in the parameter value.

Fig. 8 demonstrates that the parameters that are the most influential on the concentration of DHA is its rate of production P_{DHA} and the rate at which it is converted to 14-HpDHA by ALOX12 (k_3). The concentration of 17-HDHA is dependent upon the majority of parameters in the ALOX15 pathway (except k_6), increasing the most when P_{DHA}, the rate 17-HpDHA is metabolised to 17-HDHA by GPX4 (k_4) and the rate at which DHA is converted to 17-HpDHA by ALOX15 (k_2) increase and when k_3, the rate 17-HpDHA is converted by ALOX15 (k_7) and the rate of conversion of 17-HDHA by auto-oxidation (k_9) decrease. Similarly, the concentration of 14-HDHA is dependent upon the parameters in the ALOX12 pathway. In particular, 14-HDHA increases when P_{DHA} and the rate at which 14-HpDHA is metabolised to 14-HDHA (k_5) increase and when the rate of conversion of 14-HpDHA by ALOX5 (k_{11}), the degradation rate constant of 14-HDHA (δ_5) and the rate of conversion of 14-HpDHA by ALOX12 (k_{10}) decrease.

All oxylipin concentrations are sensitive to P_{DHA} which explains the poor fit for some participants in Fig. 6 between simulated and measured concentrations of DHA derived using a constant value for P_{DHA}.

4.1.2. Uncertainty analysis

As discussed in Section 3, the rate parameters encompass the complicated relationship between the enzyme activity and corresponding gene expression. It is likely that they vary for each individual i.e. they are not just a biochemical constant that is independent of other factors. Medication taken by participants in the cohort and polymorphisms in the genes will both influence the kinetics. We therefore wish to determine, firstly, the global effect of the parameters and, secondly, the effect of variations in gene expression on the bioactive oxylipin concentrations to assess the uncertainty of the simulated value.

Using the mRNA levels from each participant in our cohort, we solve our system of algebraic equations, drawing a Latin Hypercube sample from the range of values determined by doubling and halving each of the parameters in Table 8 using the function maximinLHS in R. The resulting predicted values of DHA, 17-HDHA and 14-HDHA in this parameter space are demonstrated in Fig. 9.

We observe from Fig. 9 that the experimentally measured concentrations of DHA, 17-HDHA and 14-HDHA fall within the region of uncertainty predicted by the simplified model for all individuals indicating the importance of the values chosen for the parameters.
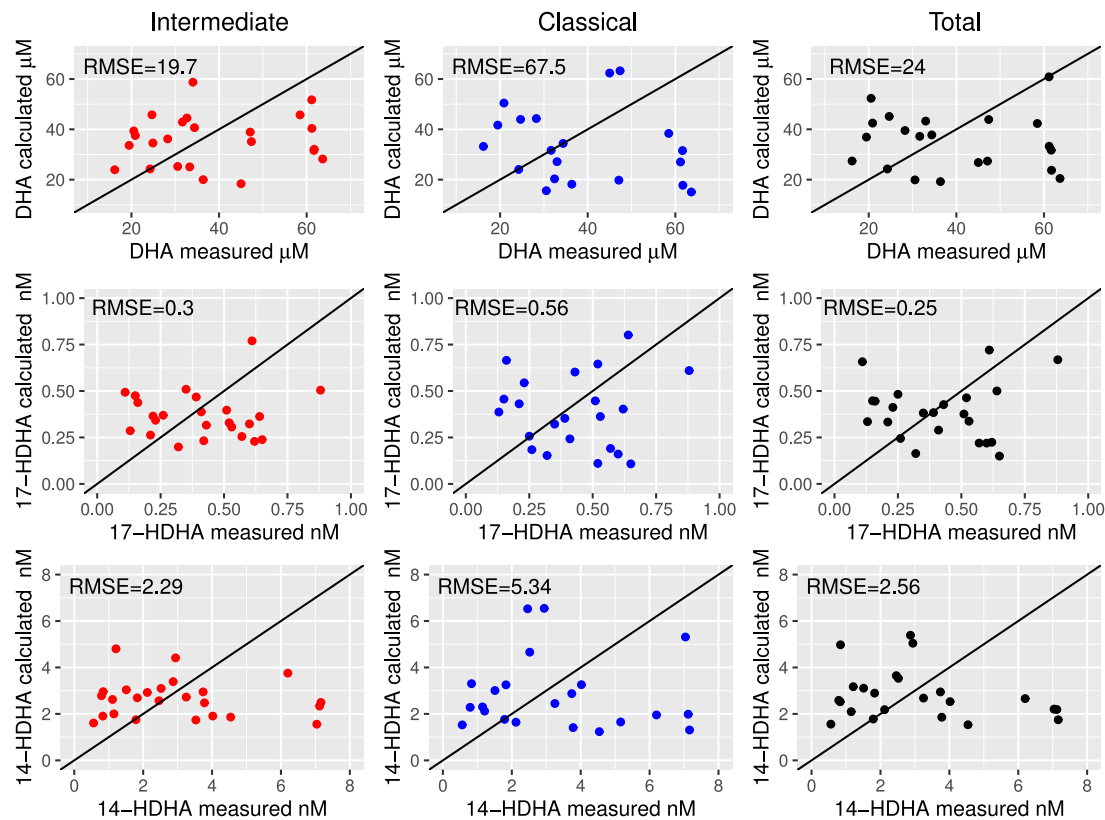
Fig. 6. A comparison between the steady state concentrations of DHA, 17-HDHA and 14-HDHA predicted from Eqs. (7)–(11) using the globally fit parameters in Table 8 and gene expression data for each individual in the cohort for intermediate (red), classical (blue) and total (black) monocytes with the experimentally measured values for the same individual.
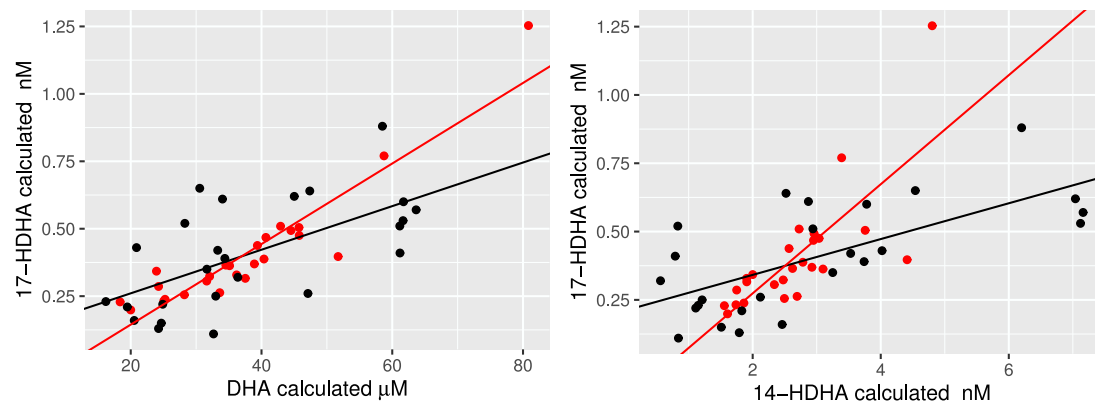

Fig. 7. The relationship between steady state concentrations of DHA and 17-HDHA and 14-HDHA and 17-HDHA predicted from the model simulations (red dots) and experimental measurements (black dots) for each individual in the cohort. The best fitting regression line for each case is denoted by the red and black lines, respectively. Eqs. (7)–(11) were solved with mRNA data for intermediate monocytes using parameter values in Table 8.

The expression of genes in the pathway is affected by many factors including inflammation, medication and other diseases. Using the parameter values in Table 8, we solve our system of algebraic equations but this time draw a Latin Hypercube sample from the range of mRNA values determined from the minimum and maximum values measured in the cohort. The predicted oxylipin concentrations are shown in Fig. 10.

The simulated results shown in the boxplots indicate that the predicted median, minimum and interquartile concentrations of DHA are similar to those observed experimentally whilst the maximum concentration predicted is higher than that measured in the cohort. The 25th percentile, minimum and maximum values predicted for 17-HDHA are similar to those in the cohort but the median and 75th percentile are

both underpredicted in the simulations. Similarly, the range of 14-HDHA is under predicted compared with the cohort, suggesting that the variation of gene expression values used is not enough to anticipate the physically relevant outcomes or that other mechanisms, not included in the model, are important.

4.2. Model predictions

In the previous sections, we have used the experimental data to create the model and ascertain the model parameters. We now use our model to examine two scenarios that have not been looked at experimentally, namely the effects of up- and down-regulation of genes on the oxylipin concentrations, and the impact of theoretical dosing with 17-HDHA on metabolic products down-stream of 17-HDHA.
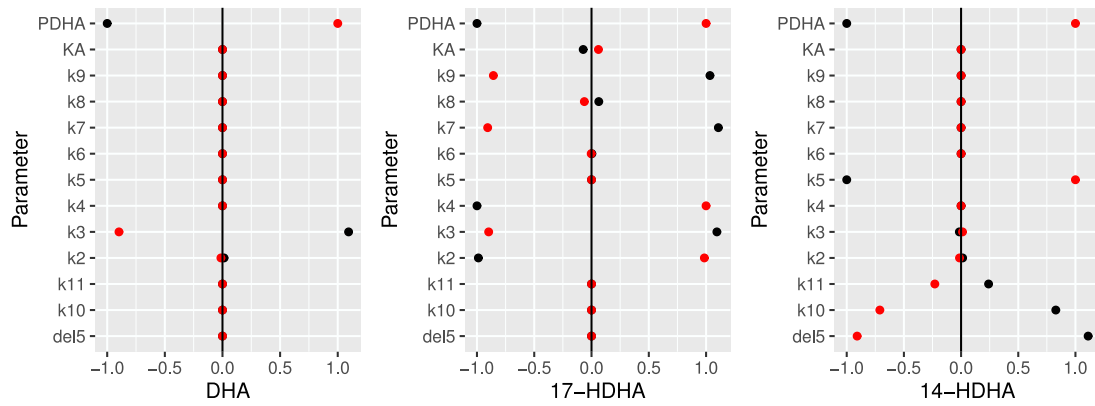
Fig. 8. The effect of varying parameter values on the steady state concentrations of DHA, 17-HDHA and 14-HDHA. Baseline parameter values for intermediate monocytes are taken from Table 8 and each parameter is sequentially varied by a 10% decrease (black) and a 10% increase (red).
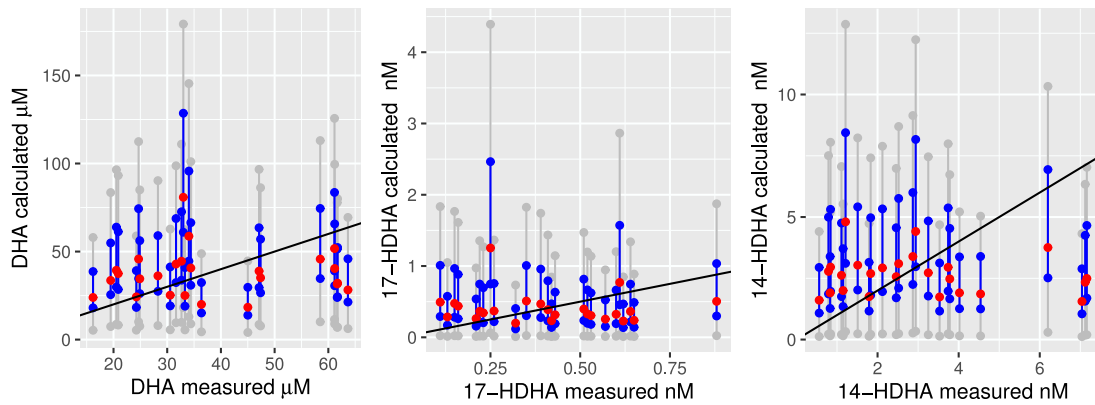

Fig. 9. A comparison of simulated and experimentally measured concentrations of DHA, 17-HDHA and 14-HDHA for each individual in our cohort using their mRNA levels and sampling parameters from the parameter space created by halving and doubling the values in Table 8 for intermediate monocytes. The red dots denote the simulated results from Fig. 6, the blue line represents the interquartile range and the grey line illustrates the 10%–90% range. The black line represents the line of equality between simulated and measured values.
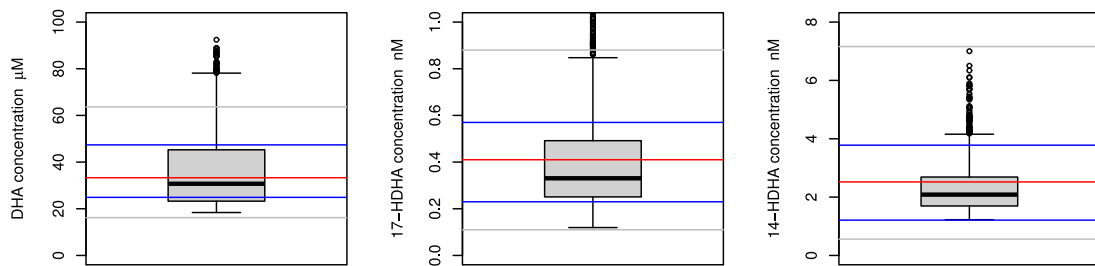

Fig. 10. A comparison of simulated (box and whisker plot) and experimentally measured (full width horizontal lines) concentrations of DHA, 17-HDHA and 14-HDHA using the parameter values in Table 8 for intermediate monocytes and sampling mRNA levels from the parameter space created by the minimum and maximum values measured in the cohort. The full width horizontal red lines are the median values of oxylipin measured in the cohort, the blue lines are the 25th and 75th percentiles and the grey lines are the minimum and maximum values measured. Horizontal lines within the box and whisker plot are the simulated median, 25th and 75th percentiles and minimum and maximum values.

4.2.1. The effect of gene expression on oxylipin concentration

The changes in gene expression during the acute and chronic phases of inflammation are complex. In [38], ALOX12, ALOX5 and ALOX15 are upregulated in regulatory T-cells when they differentiate from T-cells. Regulatory T-cells are key mediators in the resolution of inflammation, so the upregulation of these genes in this cell type might be seen towards the end of acute inflammation. Similarly, [39] suggests a similar pattern of upregulation of ALOX15 in monocyte derived macrophages as a mechanism for the initiation of the resolution of inflammation. However, for diseases involving chronic inflammation it is unclear whether it would be expected to see the same level of upregulation of these genes.

To assess the impact of changes in gene expression on the oxylipin concentrations, we solve our steady state equations given by (7)–(11). From Fig. 2, there was no correlation between the ALOX genes so we vary each gene individually defined by the range of values measured in the cohort. The effect on the resulting concentrations is shown in Fig. 11, along with the measured oxylipin concentrations and gene expression from one participant in the cohort (note that median values were not used as they do not necessarily represent the relative expressions and concentrations observed in an individual).

The model suggests that up-regulation of ALOX12 and ALOX15 results in lower concentrations of DHA, 14-HDHA and 17-HDHA. 14-HDHA and 17-HDHA are also down-regulated with increasing ALOX5.
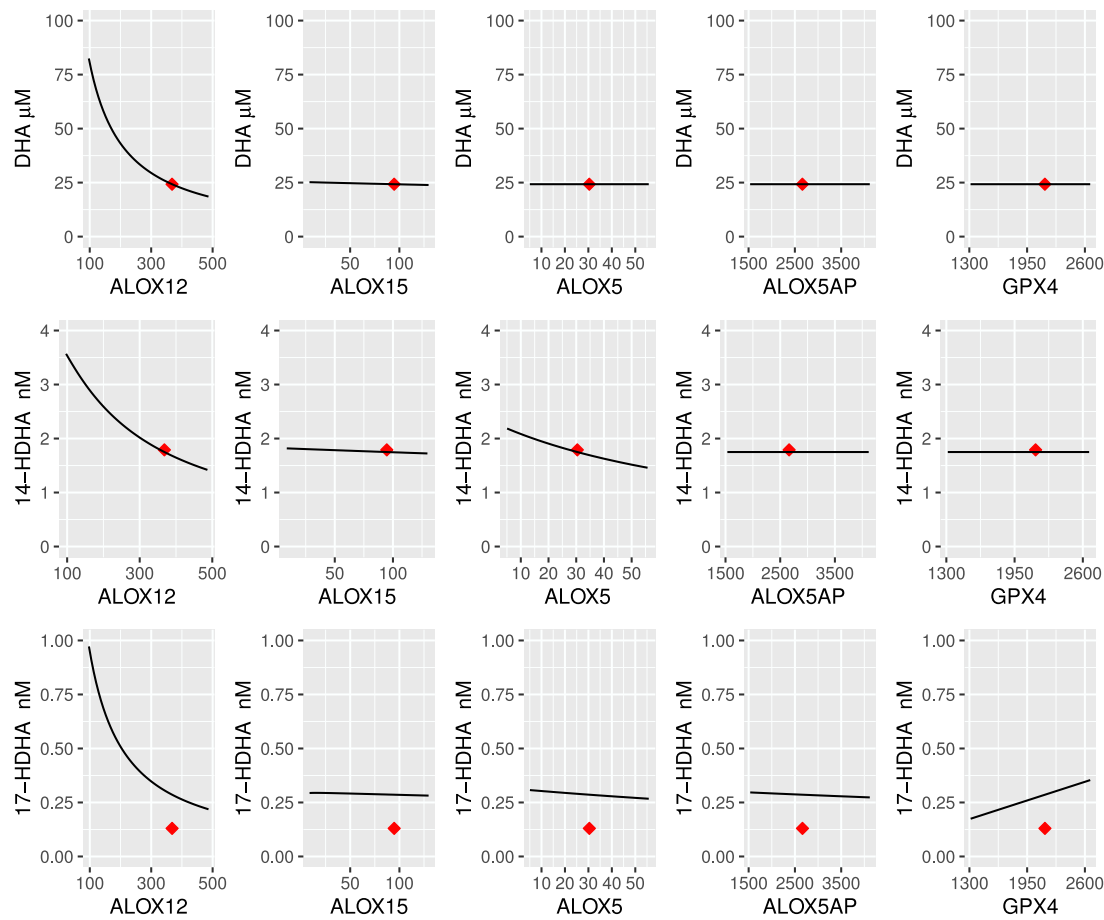
Fig. 11. The effect of varying gene expression on the predicted steady state concentrations of DHA, 17-HDHA and 14-HDHA from solving (7)–(11). Parameter values for intermediate monocytes are taken from Table 8 and each gene is sequentially varied whilst keeping the remaining genes constant. Baseline values for gene expression are taken from one participant in the cohort and the red diamonds represent the actual measured gene expression and oxylipin concentrations for that participant i.e. [DHA] = 24.25 μM, [14-HDHA] = 1.79 nM, [17-HDHA] = 0.13 nM, ALOX12 = 368, ALOX15 = 94.7, ALOX5 = 30.4, ALOX5AP = 2663, GPX4 = 2150.

An increase in expressions of GPX4 and ALOX5AP up- and down-regulate 17-HDHA, respectively. Lower levels of 17-HDHA have been associated with higher perceived pain and are likely to result in lower concentrations of the D-series resolvins suggesting that it will take longer for inflammation to resolve. ALOX12 is a biosynthetic enzyme of lipoxin which is a transmitter that enhances the host's defence against infections by triggering inflammation [40]. Fig. 11 shows that down-regulation of ALOX12 results in higher concentrations of 14-HDHA, suggesting that individuals who have high levels of 14-HDHA might have less inflammation. This is highlighted by our outlier individual mentioned earlier (removed from our cohort), who had a significantly larger concentration of 14-HDHA than any other participants. This individual was taking a combination of NSAIDs, steroids and opioids, which might be suppressing the inflammation.

The baseline values for gene expression taken from the one participant in the cohort, and used in the simulations, gave good agreement between measured and simulated concentrations of DHA and 14-HDHA. However, actual concentrations of 17-HDHA were lower than those predicted.

4.2.2. Dosing with 17-HDHA

In animal studies, dosing with 17-HDHA reversed pain behaviour in a model of OA pain [15]. To explore the processes for these observations, we consider the downstream products of 17-HDHA i.e. the D series resolvins RvD3, RvD4, RvD5 and RvD6 as illustrated in Fig. 12.

We use our model to simulate a theoretical dosing regime in human participants and examine how the concentration of resolvins change over time. We assume that 17-HDHA is administered as a single dose,
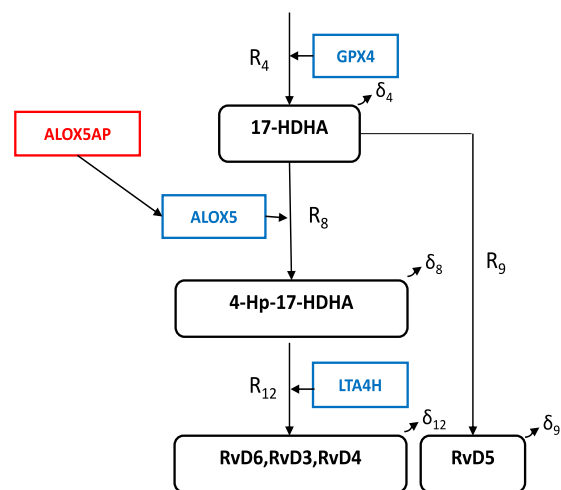

Fig. 12. The metabolism of 17-HDHA into the resolvins RvD3, RvD4, RvD5 and RvD6 taken from Fig. 1.

concentration D_{17} into the blood at time t_d (a time after all of the oxylipin concentrations are at homeostatic levels) so that the concentration at $t = t_d$ is given by

$$[\text{17-HDHA}] = [\text{17-HDHA}]_{ss} + D_{17}$$

Table 9

Rate terms for the resolvins model shown in Fig. 12 and expressed in Eqs. (15)–(17). [ ] denotes the oxylipin concentration and enzyme concentration. Rate constants are denoted by k.

Rate	Description	Term
R_8	Conversion of 17-HDHA by 5-LOX (activated by FLAP)	$k_8 \left(1 + \frac{ALOX5AP}{K_A}\right) ALOX5[\text{17-HDHA}]$
R_9	Conversion of 17-HDHA by auto-oxidation	$k_9[\text{17-HDHA}]$
R_{12}	Conversion of 4-Hp-17-HDHA by LTA4H	$k_{12}LTA4H[\text{4-Hp-17-HDHA}]$

Table 10

Parameter values determined from the steady state equations (19)–(21) using values for k_8 and k_9 from Table 8 for intermediate monocytes.

Parameter	Fitted value	Units	Parameter	Fitted value	Units
k_8	1×10^{-9}	s^{-1}	δ_9	147.6×10^{-4}	s^{-1}
k_9	9×10^{-4}	s^{-1}	δ_{12}	3.18×10^{-4}	s^{-1}
k_{12}	0.019×10^{-4}	s^{-1}			

where $[\text{17-HDHA}]_{ss}$ is the concentration of 17-HDHA at steady state before dosing.

We focus on the ALOX15 pathway including the following equations into the mathematical model given by Eqs. (1)–(5) to explore the responses downstream of 17-HDHA.

$$\frac{d[\text{4-Hp-17-HDHA}]}{dt} = R_8 - R_{12} - \delta_8[\text{4-Hp-17-HDHA}], \qquad (15)$$

$$\frac{d[\text{RvD5}]}{dt} = R_9 - \delta_9[\text{RvD5}], \qquad (16)$$

$$\frac{d[\text{RvD3,4,6}]}{dt} = R_{12} - \delta_{12}[\text{RvD3,4,6}], \qquad (17)$$

A reminder of the rate terms R_8, R_9 and the definition of R_{12} is provided in Table 9 and initial conditions at $t = 0$ are

$$[\text{4-Hp-17-HDHA}]_0 = [\text{4-Hp-17-HDHA}]_{ss}, \quad [\text{RvD5}]_0 = [\text{RvD5}]_{ss},$$

$$[\text{RvD3,4,6}]_0 = [\text{RvD3,4,6}]_{ss}, \qquad (18)$$

where $[]_0$ is the initial concentration of oxylipin and subscript ss denotes the concentration at steady state.

As before, we assume that the decay rate constants of the intermediate metabolites are negligible as the majority of the oxylipin is enzymatically converted i.e. $\delta_8 = 0$ so at steady state i.e. $\frac{d}{dt} = 0$, Eqs. (15)–(17) can be reduced to the algebraic system

$$0 = k_8 \left(1 + \frac{ALOX5AP}{K_A}\right) ALOX5[\text{17-HDHA}]$$
$$- k_{12}LTA4H[\text{4-Hp-17-HDHA}], \qquad (19)$$

$$0 = k_9[\text{17-HDHA}] - \delta_9[\text{RvD5}], \qquad (20)$$

$$0 = k_{12}LTA4H[\text{4-Hp-17-HDHA}] - \delta_{12}[\text{RvD3,4,6}]. \qquad (21)$$

We do not have any measurements from our participants for 4-Hp-17-HDHA as there are no reference standards or RvD3,4,5,6 as they are below the lower limit of quantification (LLOQ), namely 50pM. The LLOQ for 4-Hp-17-HDHA is also not known. However, in order to proceed, we assume that the concentration of RvD5 for each participant is 50% of its LLOQ value i.e. 25 pM and for RvD3,4,6, the same percentage for each but taking the sum of these three values i.e. 75 pM. We assume that the concentration of 4-Hp-17-HDHA is mid-way between the concentration of 17-HDHA and RvD3,4,6 i.e. 0.23 nM. This then allows us to estimate the parameters k_{12}, δ_9 and δ_{12} (see Table 10) from the steady state Eqs. (19)–(21) using the values determined in Table 8 for k_8 and k_9 and the median expression of genes LTA4H, ALOX5 and ALOX5AP in the cohort.

In [18], 17-HDHA and RvD4 (and other oxylipins) were measured in SARS-CoV-2 patients and there was a strong positive correlation found between 17-HDHA and RvD4 (RvD3, RvD5 and RvD6 were not measured). This is also highlighted from the model Eqs. (20)–(21)

where at steady state, RvD5 and RvD3,4,6 are both linearly dependent on 17-HDHA.

We assume that mRNA levels remain unchanged after dosing as the timescale that gene changes occur tend to be of the order of days. We solve the system of ODEs given by Eqs. (1)–(5) and (15)–(17) using the ode solver in R with the default integrator lsoda. Parameter values are given in Tables 8 (intermediate) and 10 and the median mRNA values for the cohort are used to examine the effect on 17-HDHA and the resolvins for different dosing concentrations ranging from a dose of 0.01 nM–1 μM of 17-HDHA administered as a single dose. The resulting oxylipin concentrations before and after dosing are shown in Fig. 13a–c.

There is a steep increase in all of the concentrations after administration of 17-HDHA before returning to pre-dosing levels. 17-HDHA (Fig. 13a), and RvD5 (Fig. 13c) quickly decay after approximately 2 h but RvD3,4,6 (Fig. 13b) takes longer to return to its homeostatic levels (approximately 10 h) indicating that dosing with 17-HDHA increases the production of resolvins which may help to down-regulate the inflammatory response, allowing a return to tissue homeostasis. The increase in concentration of RvD5 is much higher than RvD3,4,6 suggesting that results initially favour the RvD5 biosynthesis pathway, as also suggested by [14]. Animal dosing studies (from within our group, yet to be published) administering a single dose of 17-HDHA showed an approximately 4-fold increase in plasma 17-HDHA levels post-dose. A similar 4-fold increase in 17-HDHA is predicted in Fig. 13a for a dose of 1 nM. However, there is no time-course data from animal studies regarding how long the additional 17-HDHA remains in the blood before returning to pre-dose steady state levels. In [15] it was observed that pain behaviour improves for around 4 h post dose before returning to pre-dose levels and this approximately corresponds to the time that RvD34,6 is as its highest i.e. (>0.072 nM).

Plots of the maximum concentrations following dosing and the time for the concentrations of 17-HDHA, RvD5 and RvD3,4,6 to reach their LLOQ (RvD5 and RvD3,4,6 only) are shown in Fig. 14a–c.

The maximum concentration of 17-HDHA, 4-Hp-17-HDHA, RvD3, 4,6 and RvD5 after dosing with 17-HDHA was linearly correlated with dose. The concentration of resolvins can only be measured experimentally if they are greater than their detectable levels. The time taken for RvD5 to reach its LLOQ of 50pM is approximately 6 times quicker than for RvD3,4,6 to reach its levels of 150pM for all doses > 0.1 μM. However, the simulations indicate that the concentrations of the resolvins do not reach the detectable levels when dosed with low levels of 17-HDHA i.e. < 0.1 μM (RvD3,4,6) and <10 nM (RvD5), suggesting that plasma samples from individuals with typical concentrations of 17-HDHA will have immeasurable resolvins levels with current experimental methods. This is consistent with what is observed experimentally, highlighting the analytical challenge for many laboratories of quantifying biosamples and consistently reproducing results for low endogenous concentrations of SPMs, as they are only appear to be detectable with current methods, when the concentration of the precursor 17-HDHA is large [15,18]. With further validation, a mathematical modelling approach to determining levels of SPMs, based on the levels of their precursors (which are routinely measured experimentally), could be a potential solution to this issue.
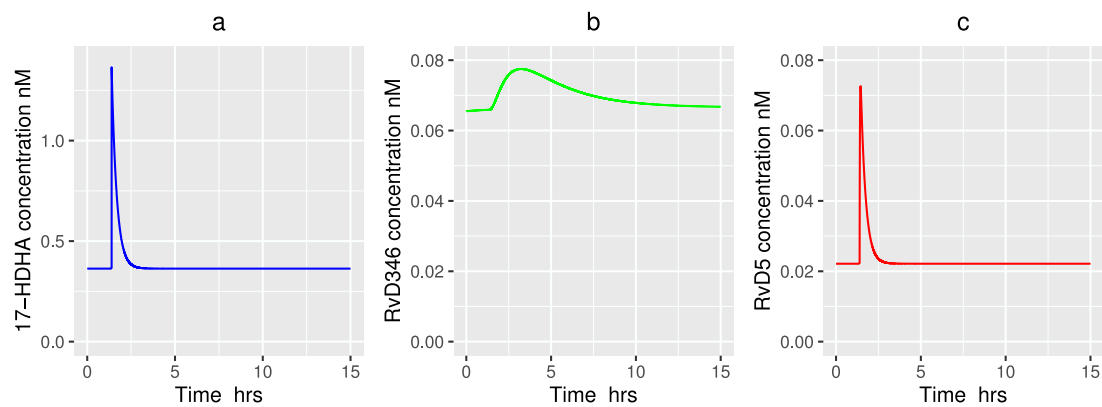
Fig. 13. Model simulations of Eqs. (1)–(5) and (15)–(17) illustrating the concentrations of 17-HDHA (blue), RvD3,4,6 (green) and RvD5 (red) in nM before and after dosing with 1 nM 17-HDHA at time $t = 5000$ s ($\approx$1.4 h). Parameter values are taken from Tables 8 for intermediate monocytes and 10 and mRNA levels are assumed to be the median values measured in the cohort.
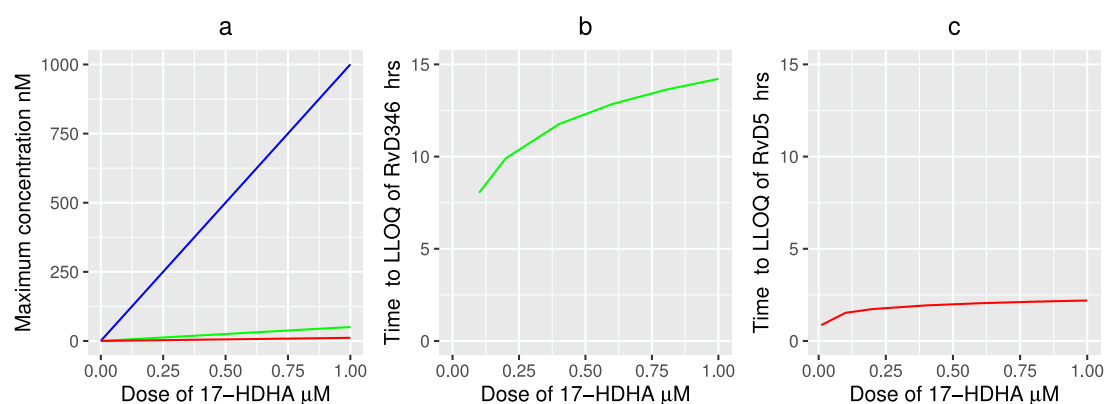

Fig. 14. (a) The maximum concentrations predicted by Eqs. (1)–(5) and (15)–(17) of 17-HDHA (blue), RvD3,4,6 (green) and RvD5 (red) with increasing doses of 17-HDHA of 0.01 nM–1 μM. Time in hours for (b) RvD3,4,6 (green) and (c) RvD5 (red) to reach their LLOQ after dosing with increasing doses of 17-HDHA. Parameter values are taken from Tables 8 for intermediate monocytes and 10 and mRNA levels are assumed to be the median values measured in the cohort.

5. Discussion

The metabolic pathway for DHA is relatively well defined, and our mathematical model incorporates established aspects of the pathway. This does not include any feedback in regulation of inflammatory mediators since none are known at present, though future models can be amended to incorporate this as well as alternative pathways for resolvins that have recently been suggested [13,14]. Using bioactive oxylipin concentrations and gene expression data from participants with OA pain, the principal aim of this study was to develop a novel mathematical model to describe how differences in enzymatic pathways (and their corresponding genes) may affect the concentration of the associated bioactive products. Of particular interest, were the differences that affect the concentration of 17-HDHA, which has been associated with OA pain in previous studies [11].

Mathematical modelling of metabolic networks can often lead to large number of ODEs governed by many parameters that are often not measurable or straightforward to estimate from experimental data. To address this, disparate experimental datasets were utilised above in developing a kinetic model of DHA metabolism. From this we were able to reduce the full DHA pathway to include only those metabolites which had been measured without disturbing the network shape surrounding them. In conjunction with steady state concentrations of oxylipins and gene expression data, we made some simplifying assumptions in relation to the biology to facilitate full parameterisation of the ODE model of the reduced DHA pathway.

One such simplification was our choice to model the reactions linearly despite the known enzymatic kinetic data (albeit for a different cell type under *in vitro* conditions and the assumption that gene expression and enzyme concentration are proportional). It was shown that this assumption resulted in a significantly better fit between the model predictions and the measured concentrations in the cohort for DHA, mainly due to the increased sensitivity of the model to the input parameter P_{DHA} for non-linear choices. This may reflect the presence of additional currently unknown factors involved in converting enzyme concentrations into the mRNA levels used in the simulations and warrants further investigation.

Using mRNA levels measured from monocytes isolated from whole blood samples for each individual in our cohort, the model simulates the concentration of oxylipins in the DHA pathway. However, the model is sensitive to the choice of parameters and it is likely that values are different for each individual depending upon their environment, stress, inflammation, diet and medications. A comparison with a control cohort of healthy individuals would be useful in determining the impact of some of these factors on the parameters.

Our model results examined the qualitative relationships between the oxylipin concentrations. There is some agreement between measured and simulated plasma concentrations but a better understanding of the parameters which govern the concentrations of 17-HDHA and 14-HDHA is essential for more accurate predictions. The oxylipin concentrations measured experimentally are a combination of the oxylipins produced by the different cell types which have been transported outside of the cells. We observed that the simulated results vary depending on whether intermediate or classical mRNA levels have been input into the model so further study of the relative contribution of genes from the different cell types would be valuable.

Despite our simplifying assumptions, the model is able to predict qualitative behaviour consistent with that observed experimentally,
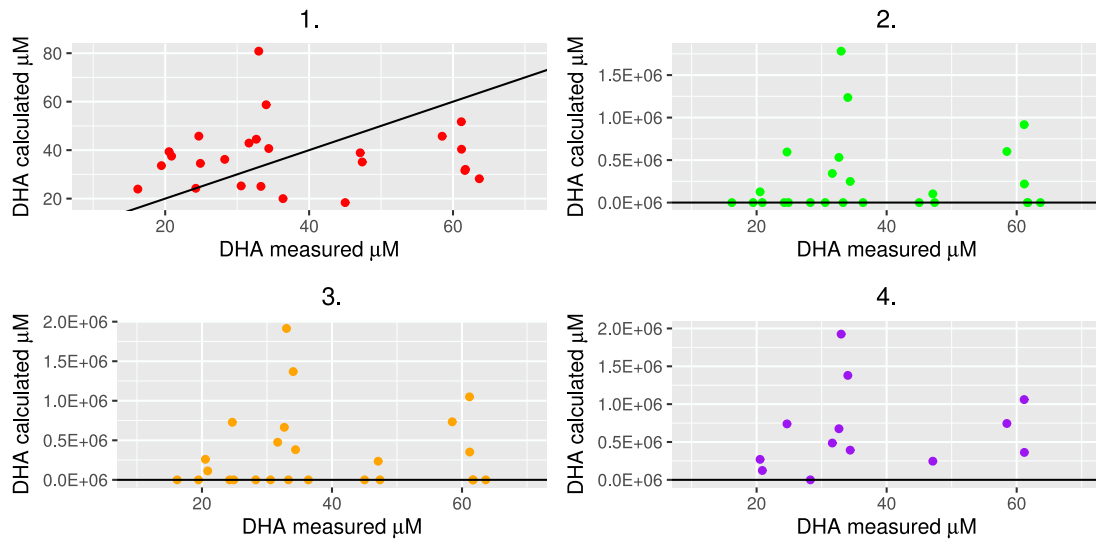
Fig. 15. A comparison between the steady state concentrations of DHA predicted from Eq. (A.5) using the values for $k_{cat_{15}}$, $k_{cat_{12}}$, $K_{m_{15}}$ and $K_{m_{12}}$ in Table 7 and gene expression data for each individual in the cohort for intermediate monocytes for forms of R_2 and R_3 given by Eqs. (A.1)–(A.4) with the experimentally measured values for the same individual.

and our attempt to understand the relationships between the oxylipin concentrations and expression of genes has highlighted the need for future experimental studies. Our model has shown that upregulation of some anti-inflammatory genes such as ALOX, results in lower levels of 17-HDHA, potentially increasing perceived pain and increasing time to resolution. It has also shown that dosing with 17-HDHA increases the concentration of resolvins, which may help to down-regulate the inflammatory response. Analysis of mRNA levels at intervals after dosing with 17-HDHA would clarify their time dependent behaviour and the presence of feedback loops within the pathway.

The model has identified several areas where more targeted experiments would be useful to improve the model accuracy in predicting oxylipin concentrations from mRNA levels measured in individuals. A validated model has the potential to provide a more cost-effective option to costly experiments, allowing the effect of, for example, therapeutic targets to be investigated. However, the DHA pathway is just one part of a much wider network involving pro and anti-inflammatory interactions and should not be considered in isolation. Similarly, 17-HDHA is just one oxylipin that has been shown to be involved in the pain experienced in individuals with OA. However, it is more likely to be a combination of oxylipins and enzymes interacting together that influences the pain experienced. Examining DHA metabolism alongside other important pathways would be an interesting future study and might provide insight into why some OA patients are more likely to experience chronic pain.

CRediT authorship contribution statement

S.J. Franks: Writing – original draft, Methodology, Investigation. **P.R.W. Gowler:** Data curation. **J.L. Dunster:** Writing – review & editing. **J. Turnbull:** Writing – review & editing, Data curation. **S.A. Gohir:** Data curation. **A. Kelly:** Data curation. **A.M. Valdes:** Data curation. **J.R. King:** Writing – review & editing, Supervision, Methodology. **D.A. Barrett:** Data curation. **V. Chapman:** Writing – review & editing, Supervision, Methodology, Funding acquisition, Data curation. **S. Preston:** Writing – review & editing, Supervision, Methodology.

Declaration of competing interest

We have no conflicts of interest to disclose.

Data availability

I have shared my code at the "Attach File" step.

Appendix A. Alternative kinetic models

The form of R_2 and R_3 presented by Eq. (12) and alternative forms more consistent with the steady state kinetic data in Table 7 to predict the concentration of DHA are

1. Linear forms for R_2 and R_3

$$R_2 = \frac{k_{cat_{15}}\alpha_{15}}{K_{m_{15}} + [\text{DHA}]_m}[\text{DHA}], \qquad R_3 = \frac{k_{cat_{12}}\alpha_{12}}{K_{m_{12}} + [\text{DHA}]_m}[\text{DHA}].$$
(A.1)

2. Michaelis–Menten for both reactions

$$R_2 = \frac{k_{cat_{15}}\alpha_{15}\text{ALOX15}_m[\text{DHA}]}{K_{m_{15}} + [\text{DHA}]}, \qquad R_3 = \frac{k_{cat_{12}}\alpha_{12}\text{ALOX12}_m[\text{DHA}]}{K_{m_{12}} + [\text{DHA}]}.$$
(A.2)

3. Michaelis–Menten for R_2 and saturation kinetics for R_3

$$R_2 = \frac{k_{cat_{15}}\alpha_{15}\text{ALOX15}_m[\text{DHA}]}{K_{m_{15}} + [\text{DHA}]}, \qquad R_3 = k_{cat_{12}}\alpha_{12}\text{ALOX12},$$
(A.3)

4. Saturation kinetics for both R_2 and R_3

$$R_3 = k_{cat_{15}}\alpha_{15}\text{ALOX15}, \qquad R_3 = k_{cat_{15}}\alpha_{15}\text{ALOX12}, \qquad (A.4)$$

P_{DHA_M} is determined from the steady state equation analogous to Eq. (7) i.e.

$$P_{DHA_M} = R_2 + R_3, \qquad (A.5)$$

where R_2 and R_3 are defined by Eqs. (A.1)–(A.4). Using the values for $k_{cat_{15}}$, $k_{cat_{12}}$, $K_{m_{15}}$ and $K_{m_{12}}$ in Table 7 and the measured concentrations of DHA in the cohort, P_{DHA_M} is calculated to be for 1. $0.15 \leq P_{DHA_M} \leq 0.92$ (median 0.37), 2. $0.156 \leq P_{DHA_M} \leq 0.69$ (median 0.347), 3. $0.16 \leq P_{DHA_M} \leq 0.71$ (median 0.36) and 4. $0.168 \leq P_{DHA_M} \leq 0.718$ (median 0.361) for intermediate monocytes.
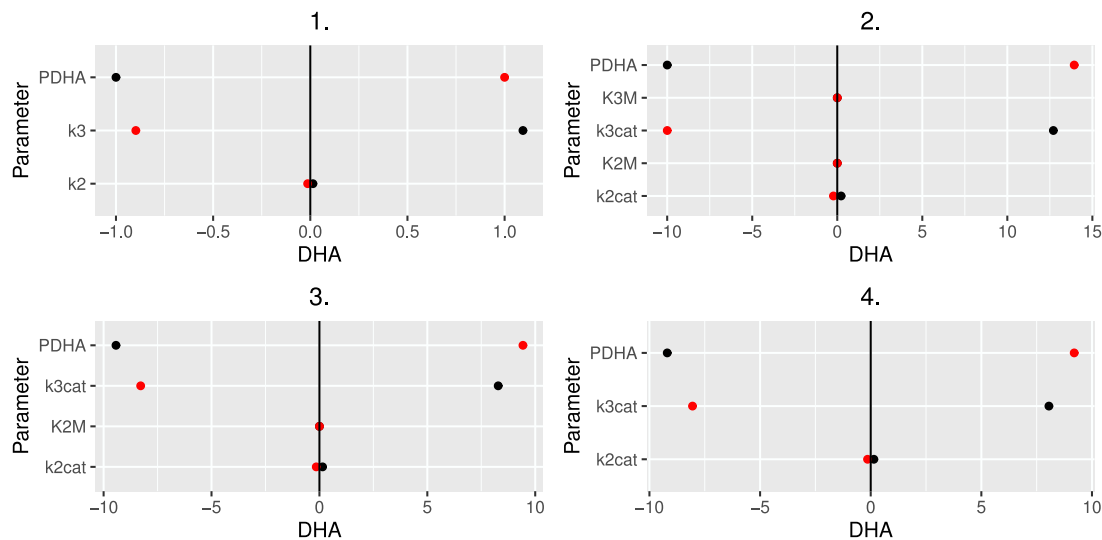
Fig. 16. The effect of varying parameter values on the steady state concentrations of DHA for intermediate monocytes for the forms for R_2 and R_3 given by Eqs. (A.1)–(A.4). Baseline parameters are taken from Table 7 and P_{DHA} is taken to be the median value.

The concentrations of DHA calculated from solving the algebraic Eq. (A.5) for each individual using parameter values in Table 7, the median value of P_{DHA_M} and the gene expression for each individual in our cohort is shown in Fig. 15 for intermediate monocytes for each of the forms of R_2 and R_3 described above.

Fig. 15 indicates that the linear form of R_2 and R_3 gives a significantly better fit between the model predictions and the measured concentrations in the cohort for DHA. Performing a local sensitivity analysis, as detailed in Section 4.1.2, Fig. 16 shows that the concentration of DHA is very sensitive to P_{DHA} and $k_{3_{cat}}$ for forms of R_2 and R_3 given by Eqs. (A.2)–(A.4). For these cases, the concentration of DHA increases approximately 10 times any increase in the parameter suggesting such expressions are unlikely to reflect reality, and explaining the poor fit between simulated and measured concentrations when using the median value of P_{DHA}.

Appendix B. Supplementary data

Supplementary material related to this article can be found online at https://doi.org/10.1016/j.mbs.2024.109228.

References

[1] C.N. Serhan, Pro-resolving oxylipin mediators are leads for resolution physiology, Nature 510 (7503) (2014) 92–101, http://dx.doi.org/10.1038/nature13479.

[2] D.W. Gilroy, D. Bishop-Bailey, Oxylipin mediators in immune regulation and resolution, Br. J. Pharmacol. 176 (2019) 1009–1023, http://dx.doi.org/10.1111/bph.14587.

[3] A. Recchiuti, D. Mattoscio, E. Isopi, Roles, actions, and therapeutic potential of specialized pro-resolving oxylipin mediators for the treatment of inflammation in cystic fibrosis, Front. Pharmacol. 10 (2019) http://dx.doi.org/10.3389/fphar.2019.00252.

[4] A. Oeckinghaus, S. Ghosh, The NF-kappaB family of transcription factors and its regulation, Cold Spring Harb. Perspect. Biol. 1 (4) (2009) http://dx.doi.org/10.1101/cshperspect.a000034.

[5] S.T. Smale, G. Natoli, Transcriptional control of inflammatory responses, Cold Spring Harb. Perspect. Biol. 6 (11) (2014) http://dx.doi.org/10.1101/cshperspect.a016261.

[6] D.J. Stumpo, W.S. Lai, P.J. Blackshear, Inflammation: cytokines and RNA-based regulation, Wiley Interdiscip. Rev. RNA 1 (1) (2010) 60–80, http://dx.doi.org/10.1002/wrna.1.

[7] T.H. Zaninelli, V. Fattori, W.A. Verri Jr., Harnessing inflammation resolution in arthritis: Current understanding of specialized pro-resolving oxylipin mediators' contribution to arthritis physiopathology and future perspectives, Front. Physiol. 12 (2021) http://dx.doi.org/10.3389/fphys.2021.729134.

[8] P.F. Duffney, M.L. Falsetta, A.R. Rackow, T.H. Thatcher, R.P. Phipps, P.J. Sime, Key roles for lipid mediators in the adaptive immune response, J. Clin. Invest. 128 (7) (2018) 2724–2731, http://dx.doi.org/10.1172/JCI97951.

[9] J. Rossaint, A. Margraf, A. Zarbock, Role of platelets in leukocyte recruitment and resolution of inflammation, Front. Immunol. 9 (2018) http://dx.doi.org/10.3389/fimmu.2018.02712.

[10] D. Furman, J. Campisi, E. Verdin, P. Carrera-Bastos, S. Targ, C. Franceschi, L. Ferrucci, D.W. Gilroy, A. Fasano, G.W. Miller, A.H. Miller, A. Mantovani, C.M. Weyand, N. Barzilai, J.J. Goronzy, T.A. Rando, R.B. Effros, A. Lucia, N. Kleinstreuer, G.M. Slavich, Chronic inflammation in the etiology of disease across the life span, Nature Med. 25 (2019) 1822–1832, http://dx.doi.org/10.1038/s41591-019-0675-0.

[11] A.M. Valdes, S. Ravipati, C. Menni, A. Abhishek, S. Metrustry, J. Harris, A. Nessa, F.M.K. Williams, T.D. Spector, M. Doherty, V. Chapman, D.A. Barrett, Association of the resolvin precursor 17-HDHA, but not D- or E- series resolvins, with heat pain sensitivity and osteoarthritis pain in humans, Sci. Rep. 7 (2017) http://dx.doi.org/10.1038/s41598-017-09516-3.

[12] C.N. Serhan, S.K. Gupta, M. Perretti, C. Godson, E. Brennan, Y. Li, O. Soehnlein, T. Shimizu, O. Werz, V. Chiurchiu, A. Azzi, M. Dubourdeau, S.S. Gupta, P. Schopohl, M. Hoch, D. Gjorgevikj, F.M. Khan, et al., The atlas of inflammation resolution (AIR), Mol. Aspects Med. 74 (2020) http://dx.doi.org/10.1016/j.mam.2020.100894.

[13] S.C. Perry, C. Kalyanaraman, B.E. Tourdot, W.S. Conrad, O. Akinkugbe, J.C. Freedman, M. Holinstat, M.P. Jacobson, T.R. Holman, 15-Lipoxygenase-1 biosynthesis of 7S, 14S-diHDHA implicates 15-lipoxygenase-2 in biosynthesis of resolvin D5, J. Oxylipin Res. 61 (7) (2020) 1087–1103, http://dx.doi.org/10.1194/jlr.RA120000777.

[14] O. Radmark, Formation of eicosanoids and other oxylipins in human macrophages, Biochem. Pharmacol. 204 (2022) 115210, http://dx.doi.org/10.1016/j.bcp.2022.115210.

[15] J. Huang, J.J. Burston, L. Li, S. Ashraf, P.I. Mapp, A.J. Bennett, S. Ravipati, P. Pousinis, D.A. Barrett, B.E. Scammell, V. Chapman, Targeting the D series resolvin receptor system for the treatment of osteoarthritis pain, Arthritis Rheumatol. 69 (2017) 996–1008, http://dx.doi.org/10.1002/art.40001.

[16] D. Loukov, S. Karampatos, M.R. Maly, D.M.E. Bowdish, Monocyte activation is elevated in women with knee-osteoarthritis and associated with inflammation, BMI and pain, Osteoarthr. Cartil. 26 (2) (2018) 255–263, http://dx.doi.org/10.1016/j.joca.2017.10.018.

[17] S.A. Gohir, P. Greenhaff, A. Abhishek, A.M. Valdes, Evaluating the efficacy of internet-based exercise programme aimed at treating knee osteoarthritis (iBEAT-OA) in the community: a study protocol for a randomised controlled trial, BMJ Open 9 (10) (2019) http://dx.doi.org/10.1136/bmjopen-2019-030564.

[18] J. Turnbull, R. Jha, C.A. Ortori, E. Lunt, P.J. Tighe, W.L. Irving, S.A. Gohir, D.H. Kim, A.M. Valdes, A.W. Tarr, D.A. Barrett, V. Chapman, Serum levels of pro-inflammatory oxylipin mediators and specialised pro-resolving molecules are increased in SARS-CoV-2 patients and correlate with markers of the adaptive immune response, J. Infect. Dis. (2022) http://dx.doi.org/10.1093/infdis/jiab632.

[19] A. Wong, D.R. Sagar, C.A. Ortori, D.A. Kendall, V. Chapman, D.A. Barrett, Simultaneous tissue profiling of eicosanoid and endocannabinoid lipid families in a rat model of osteoarthritis, J. Lipid Res. 55 (9) (2014) 1902–1913, https://www.doi.org/10.1194/jlr.M048694.

[20] B. Balestrieri, D. Di Costanzo, D.F. Dwyer, Macrophage-mediated immune responses: From fatty acids to oxylipins, Molecules 27 (1) (2021) 152, http://dx.doi.org/10.3390/molecules27010152.

[21] T.S. Kapellos, L. Bonaguro, I. Gemund, N. Reusch, A. Saglam, E.R. Hinkley, J.L. Schultze, Human monocyte subsets and phenotypes in major chronic inflammatory diseases, Front. Immunol. 10 (2019) 2035, http://dx.doi.org/10.3389/fimmu.2019.02035.

[22] P. Sampath, K. Moideen, U.D. Ranganathan, R. Bethunaickan, Monocyte subsets: Phenotypes and function in tuberculosis infection, Front. Immunol. 9 (2018) http://dx.doi.org/10.3389/fimmu.2018.01726.

[23] https://hbctraining.github.io/DGE_workshop/lessons/02_DGE_count_normalization.html.

[24] C. Buccitelli, M. Selbach, mRNAs, proteins and the emerging principles of gene expression control, Nat. Rev. Genet. 21 (2020) 630–644, http://dx.doi.org/10.1038/s41576-020-0258-4.

[25] Y. Liu, A. Beyer, R. Aebersold, On the dependency of cellular protein levels on mRNA abundance, Cell 165 (3) (2016) 535–550, http://dx.doi.org/10.1016/j.cell.2016.03.014.

[26] A.F. Domenichiello, C.T. Chen, M.O. Trepanier, P.M. Stavro, R.P. Bazinet, Whole body synthesis rates of DHA from *α*-linolenic acid are greater than brain DHA accretion and uptake rates in adult rats, J. Lipid Res. 55 (1) (2014) 62–74, http://dx.doi.org/10.1194/jlr.M042275.

[27] J. Bradbury, Docosahexaenoic acid (DHA): an ancient nutrient for the modern human brain, Nutrients 3 (5) (2011) 529–554, http://dx.doi.org/10.3390/nu3050529.

[28] N.K. Singh, G.N. Rao, Emerging role of 12/15-Lipoxygenase (ALOX15) in human pathologies, Prog. Lipid Res. 73 (2019) 28–45, http://dx.doi.org/10.1016/j.plipres.2018.11.001.

[29] R. Mashima, T. Okuyama, The role of lipoxygenases in pathophysiology; new insights and future perspectives, Redox Biol. 6 (2015) 297–310, http://dx.doi.org/10.1016/j.redox.2015.08.006.

[30] J.A. Ackermann, K. Hofheinz, M.M. Zaiss, G. Krönke, The double-edged role of 12/15-lipoxygenase during inflammation and immunity, Biochim. Biophys. Acta Mol. Cell Biol. Oxylipins 1862 (4) (2017) 371–381, http://dx.doi.org/10.1016/j.bbalip.2016.07.014.

[31] A. Kulkarni, J.L. Nadler, R.G. Mirmira, I. Casimiro, Regulation of tissue inflammation by 12-lipoxygenases, Biomolecules 11 (5) (2021) 717, http://dx.doi.org/10.3390/biom11050717.

[32] Z. Zheng, Y. Li, G. Jin, T. Huang, M. Zou, S. Duan, The biological role of arachidonic acid 12-lipoxygenase (ALOX12) in various human diseases, Biomed. Pharmacother. 129 (2020) http://dx.doi.org/10.1016/j.biopha.2020.110354.

[33] S. Tang, M. Wan, W. Huang, R.C. Stanton, Y. Xu, Maresins: Specialized proresolving oxylipin mediators and their potential role in inflammatory-related diseases, Mediators Inflamm. (2018) http://dx.doi.org/10.1155/2018/2380319.

[34] C.A. Castellano, R. Chouinard-Watkins, J.T. Brenna, B.J. Meyer, S.C. Cunnane, Does aging change docosahexaenoic acid homeostasis? Implications for the challenge to cognitive health in the elderly, OCL. 18 (4) (2011) 175–180, http://dx.doi.org/10.1684/ocl.2011.0390.

[35] Y. Qin, H. Nyheim, E.M. Haram, J.M. Moritz, S.O. Hustvedt, A novel self-micro-emulsifying delivery system (SMEDS) formulation significantly improves the fasting absorption of EPA and DHA from a single dose of an omega-3 ethyl ester concentrate, Lipids Health Dis. 16 (2017) 204, http://dx.doi.org/10.1186/s12944-017-0589-0.

[36] O. Kuda, Bioactive metabolites of docosahexaenoic acid, Biochimie 136 (2017) 12–20, http://dx.doi.org/10.1016/j.biochi.2017.01.002.

[37] N.H. Schebb, H. Kühn, A.S. Kahnt, K.M. Rund, V.B. O'Donnell, N. Flamand, M. Peters-Golden, P.J. Jakobsson, K.H. Weylandt, N. Rohwer, R.C. Murphy, G. Geisslinger, G.A. FitzGerald, J. Hanson, C. Dahlgren, M.W. Alnouri, S. Offermanns, D. Steinhilber, Formation, signaling and occurrence of specialized pro-resolving lipid mediators - what is the evidence so far? Front. Pharmacol. 13 (2022) 838782, http://www.doi.org/10.3389/fphar.2022.838782. 2.

[38] R.M. Marques, M. Gonzalez-Nunez, M.E. Walker ME, E.A. Gomez, R.A. Colas, T. Montero-Melendez, M. Perretti, J. Dalli, Loss of 15-lipoxygenase disrupts Treg differentiation altering their pro-resolving functions, Cell Death Differ. 28 (11) (2021) 3140–3160, http://dx.doi.org/10.1038/s41418-021-00807-x.

[39] R.G. Snodgrass, B. Brüne, Regulation and functions of 15-lipoxygenases in human macrophages, Front. Pharmacol. 10 (719) (2019) http://dx.doi.org/10.3389/fphar.2019.00719.

[40] Z. Zheng, Y. Li, G. Jin, T. Huang, M. Zou, S. Duan, The biological role of arachidonic acid 12-lipoxygenase (ALOX12) in various human diseases, Biomed. Pharmacother. 129 (2020) 110354, http://dx.doi.org/10.1016/j.biopha.2020.110354.